# Kent Academic Repository

**Raventós-Izard, Georgina, Potau, Josep Mª, Casado, Aroa, Pastor, Juan F and Arias-Martorell, Júlia (2023) *The morphofunctional implications of the glenoid labrum of the glenohumeral joint in hominoids.* American journal of biological anthropology .**

# The morphofunctional implications of glenoid *labrum* of the glenohumeral joint in hominoids

Georgina Raventós-Izard[1]*, Josep Mª Potau[2,3], Aroa Casado[2,3], Juan F Pastor[4], Julia Arias-Martorell[1,5]*

1 Institut Català de Paleontologia Miquel Crusafont, Universitat Autònoma de Barcelona, Edifici ICTA-ICP, c/ Columnes s/n, Campus de la UAB, 08193 Cerdanyola del Vallès, Barcelona, Spain.

2 Unit of Human Anatomy and Embryology, Faculty of Medicine, University of Barcelona, c/Casanova 143 08036, Barcelona, Spain.

3 Institut d'Arqueologia de la Universitat de Barcelona (IAUB), Faculty of Geography and History, University of Barcelona, 08001 Barcelona, Spain.

4 Museo Anatómico, Departamento de Anatomía y Radiología, Facultad de Medicina, Universidad de Valladolid, c/Ramón y Cajal 7, 47005, Valladolid, Spain.

5 School of Anthropology and Conservation, Marlowe Building, University of Kent, Canterbury, CT2 7NR, UK

*corresponding author

*Email address*: georgina.raventos@icp.cat (G. Raventós-Izard) | julia.arias@icp.cat (J. Arias-Martorell)

## Abstract

**Objectives.** A morphocline of the glenoid cavity has been used to infer differences in locomotor behaviors; however, the glenoid cavity is surrounded by the glenoid *labrum*, a fibrocartilaginous structure that could influence the functionality of the glenoid. The objectives of this study are to explore the effects of the glenoid *labrum* on the area, depth, and morphology of the glenoid cavity in primates.

**Material and Methods.** Photogrammetry was used to build 3D models of the glenoid, with and without the *labrum*, and three- (3D) and two-dimensional (2D) geometric morphometrics (GM) was applied. 2D areas were collected from zenithal images for glenoids with and without *labrum* to evaluate the availability of articular surface area.

**Results.** In the 2D GM the morphocline is present in the dry-bone sample but not with the presence of the glenoid *labrum*. In the 3D GM there are differences between species mainly concerning the depth of the glenoid cavity. 2D areas reveal that the amount of articular area of the glenoid cavity increases with the presence of the *labrum*, particularly in humans.

**Discussion.** The glenoid *labrum* changes the shape, increases the depth and the surface area of the glenoid cavity, particularly in humans. Therefore, the glenoid *labrum* might hold a functional role, increasing the stability of the glenohumeral joint of primates in general, and especially in humans.

## Keywords

Geometric morphometrics; Photogrammetry; Shoulder joint; Glenoid cavity; Apes

## 1. Introduction

The morphology of the glenohumeral (shoulder) joint reflects the locomotor and postural behavior of different taxa (Jungers, 1991); in this regard, in primates, and in particular, in apes, the glenohumeral joint has been widely used to explore the differences in locomotor behaviors (e.g., Corruccini & Ciochon, 1978; Larson & Stern, 1986; Larson, 1988; Larson, 1995; MaClatchy, Gebo, Kityo, & Pilbeam, 2000; Roberts, 1974).

The glenohumeral joint of apes—including gibbons and siamangs (hylobatids) and great apes (gorillas (*Gorilla*), chimpanzees (*Pan*), orangutans (*Pongo*), and humans (*Homo*))—has anatomical features that enable the forelimbs to be held in overhead positions that are required in locomotor activities such as suspension or vertical climbing (Ashton & Oxnard, 1964; Larson, 1988; Larson, 1995; MaClatchy et al., 2000; Roberts, 1974). These features include a cranially-oriented glenoid fossa (Ashton & Oxnard, 1964), a lateral projection of the glenohumeral joint (Ashton & Oxnard, 1964), and a small, oval, and flat articular surface of the glenoid cavity articulating with a large humeral head (Ashton & Oxnard, 1964; Fleagle, 2013; Godfrey, Sutherland, Boy, & Gomberg, 1991; Larson, 1988; Larson, 1995). The size difference in hominoids between the small glenoid fossa and the large articular surface of the humeral head is indicative of increased mobility of the glenohumeral joint in hominoids (Larson & Stern, 1986; Larson, 1988; Larson, 1993; Larson, 1995; Roberts, 1974; Rose, 1989). Furthermore, an oval glenoid cavity, which is found in hominoids, some atelines, and cursorial mammals, presents a broader dorsoventral width relative to craniocaudal length, and a moderate craniocaudal and dorsoventral curvatures, allowing a wide range of axial movements (MaClatchy et al., 2000; Roberts, 1974).

A kinematic study by Chan (2007) suggested that hominoids have less glenohumeral mobility than monkeys. Subsequent studies by the same author on shoulder mobility (Chan, 2008) have shown that a dorsally-positioned scapula may enhance pectoral girdle movement in hominoids thus making their overall arm mobility not different from monkeys—except for hylobatids which possess the highest shoulder mobility among all primates included in the study. However, no gorilla or orangutan specimens were included in the studies (Chan, 2007, 2008), therefore differences in shoulder range of motion between African and Asian apes were not taken into account (Isler, 2005). Humans, which were the best hominoid species represented in the study (Chan, 2007), have particular adaptations to forelimb manipulation behaviors, which may have an effect on the findings, especially regarding the overall glenohumeral mobility range in hominoids.

Nonhominoid primates (e.g., cercopithecoids), have a more proportionate glenoid cavity relative to the humeral head, with a larger contact area between the two structures, which limits the range of movement but favors a more stable glenohumeral joint (Larson, 1995; Rose, 1989). In addition, nonhominoid primates have a lock mechanism when the humerus is fully abducted, suggesting that the humerus is not mobile in maximally protracted position due to the blocking of a cranially-located lip of the glenoid fossa into the bicipital groove when the humerus is fully abducted (Chan, 2007). Hominoids do not exhibit a lock mechanism because their distally-situated greater tubercle makes it impossible for the non-projecting superior lip of the glenoid fossa to lock into the bicipital groove (Chan, 2007); this may be an adaptation to overhead positions of the forelimbs.

Glenoid depth depends on the morphological configuration of the fossa: oval glenoid cavities are flat craniocaudally and dorsoventrally; pear-shaped glenoids have a marked craniocaudal curvature (MaClatchy et al., 2000; Roberts, 1974), due to the presence of the superior lip. This feature may affect its contact area with the humeral head, thus flatter glenoid cavities may be indicative of a more mobile but less stable glenohumeral joint, and vice versa (Arias-Martorell, 2019). In turn, the craniocaudal curvature in pear-shaped glenoids would favor flexion/extension over axial movements (MaClatchy et al., 2000; Roberts, 1974).

No morphological features of the glenoid cavity seem to be related to sex, activity, or laterality in humans (Macias & Churchill, 2015). However, kinematics studies show that the frequency of overhead positions of the forelimbs and the range of motion of the shoulder is higher in juvenile and female hominoids, mainly due to body size (Isler, 2005). Moreover, some primate species display high degree of lateralization (i.e., handedness) (Hopkins et al., 2004; Margiotoudi et al., 2019; Morino et al., 2017). However, there is no study testing intraspecific morphological differences of the glenoid cavity in nonhuman primates therefore the influence of sex, age, and laterality in the glenoid cavity morphology it is not known.

*In vivo*, the glenoid cavity presents an additional soft-tissue structure, the glenoid *labrum* (or rim), which surrounds it in its entirety. The glenoid *labrum* is a fibrocartilaginous structure, which, due to its location on the margins of the glenoid cavity, may expand the articular surface area of the glenoid cavity, thus enabling a better contact between the glenoid and the humeral head (Arias-Martorell, 2019; Howell & Galinat, 1989). It may also affect the depth of the glenoid, making it more concave (Howell & Galinat, 1989). Despite its impact in glenoid morphology, the function of the glenoid *labrum* has been not studied in detail in nonhuman primates (Arias-Martorell, 2019).

While several studies have explored the three-dimensional morphology of the dry-bone glenoid (e.g., Arias-Martorell et al., 2015; Macias & Churchill, 2015; Young, 2008), to the best of our knowledge, the morphology of the *labrum* has not been quantified in non-human primates to date. In humans, in the clinical literature, the morphology and role of the *labrum* has been studied using Magnetic Resonance Imaging (MRI) scans (e.g., Beltran, et al., 1997). We used photogrammetry to record the 3D morphology of soft tissue (i.e., the glenoid *labrum*) since it has been widely used in the anthropological field for documentation, tool reconstruction, and skeletal modeling (e.g., Katz & Friess, 2014), even though it has never been used to record cartilage tissue.

This study explores the effects of the glenoid *labrum* regarding the function and morphology of the glenoid cavity and the glenohumeral joint. We examine how the glenoid *labrum* influences the area, depth, and shape of the glenoid cavity in primates to determine whether its presence affects the functionality of the glenohumeral joint. Additionally, this study will examine the utility of photogrammetry as a soft tissue reconstruction technique.

## 2. Material and Methods

### 2.1. Sample

Our sample consisted of frozen, non-chemically preserved cadavers of 22 primates (Table 1 and SI Table 1), comprising: humans (*Homo sapiens*, N=4), chimpanzees (*Pan troglodytes*, N=6), gibbons (*Hylobates lar*, N=1, and *Nomascus gabriellae*, N=1), siamangs (*Symphalangus syndactylus*, N=1), and cercopithecines (*Chlorocebus aethiops*, N=1, *Cercocebus atys lunulatus*, N=1, *Cercopithecus ascanius*, N=1, *Miopithecus ogouensis*, N=1, *Macaca silenus*, N=1, *Macaca* *sylvanus,* N=1, *Macaca tonkeana*, N=1, *Papio hamadryas*, N=2). We obtained the human sample from the Body Donation Service of the Faculty of Medicine of the University of Barcelona (Barcelona, Spain). We obtained the non-human primate sample from the Anatomical Museum of the University of Valladolid (Valladolid, Spain), which centralizes the processing of deceased primates from zoos and animal rescue centers from Spain. All individuals included in the study died from external causes independent of this study.

We performed dissections of the cadavers, which followed the recommendations and ethical guidelines of the University of Barcelona and the Body Donation Service. We removed all the muscles and soft tissue surrounding the glenohumeral joint, of which we carefully removed the capsule and separated the two components (the humeral head and the glenoid cavity of the scapula) as well, to expose the glenoid *labrum*. We then recorded the cartilaginous structure surrounding the glenoid cavity by taking a cloud of photographs (photogrammetry) of the scapula, with each picture taken from a slightly different angle and position (see below). The same procedure was followed for glenoid cavities without the *labrum* after removing the remaining soft tissue.

### 2.2. Photogrammetry

We took the pictures with a Canon EOS 1000D camera with 10 megapixels and a 18-15 mm lens, in automatic mode or close-up. Good overlap between pictures was obtained by moving the camera only a few centimeters between shots. The clouds or sets of pictures taken ranged in number from 17 to 101 per set. These were imported into Agisoft Metashape 1.7.3 (St. Petersburg, Russia) without any prior treatment. For building the 3D models, we generated a sparse point cloud, which we used to create 3D meshes. We were able to obtain 3D models for a subset of the sample only, comprising *Homo sapiens* (N=4), *Pan troglodytes* (N=4), *Hylobates lar* (N=1), *Nomascus gabriellae* (N=1), *Chlorocebus aethiops* (N=1), *Cercocebus atys lunulatus* (N=1), *Cercopithecus ascanius* (N=1), *Miopithecus ogouensis* (N=1), and *Papio hamadryas* (N=2) (SI Table 2).

### 2.3. Geometric morphometrics

Three-dimensional geometric morphometrics were used to explore the shape of the glenoid cavity with and without *labrum* using the 3D models obtained via photogrammetric reconstruction (N=16). For the complete sample (N=22), we performed two-dimensional geometric morphometrics using the zenithal image of each glenoid cavity with and without *labrum* extracted from the cloud of photographs obtained for photogrammetric reconstruction.

We applied two landmark protocols (SI Table 3 and Fig. 1): a protocol of six landmarks (Fig. 1A, 1C) to the 3D sample, with and without *labrum*, using Landmark Editor v. 3.0 (Wiley et al., 2005) and a protocol of eight landmarks (Fig. 1B, 1D) to the zenithal images (from the photogrammetry sets) of the glenoid cavity, with and without *labrum*, using tpsDig2 v. 2.31.8 (Rohlf, 2015). Both landmark protocols capture the glenoid cavity morphology, however, the former contemplates depth, which is a feature that can only be explored with 3D data, whereas the later puts emphasis on the contour, which is more easily recorded with 2D data.

Using the ‘Morpho’ v. 2.8 package (Schlager, 2017) in R v. 4.1.1 (R Core Team, 2021) we applied a General Procrustes Analysis (GPA) to rotate, scale (to size 1 of the centroid), and translate all shapes in each sample subset (3D, with and without *labrum*, and 2D, with and without *labrum*). We carried out a Principal Component Analyses (PCA) for each sample subset with the GPA coordinates to identify shape variation between groups (cercopithecoids, chimpanzees, hylobatids, and humans). In addition, a phylogenetically-adjusted PCA (phy-PCA) was conducted to explore the shape changes and group distribution accounting for the phylogenetic structure underlying our data (Adams et al., 2020) for each sample subset. We downloaded a molecular-based time-calibrated phylogenetic tree from 10kTrees website v. 3 (Arnold, Matthewa, & Nunn, 2010), which we used for both the phy-PCA and PGLS analyses (below).

Ordinary least-squares (OLS) regression of PC scores (PC1 and PC2) vs. log-transformed centroid size (ln CS), and phylogenetic generalized least-squares (PGLS; Adams, 2014) of species mean coordinates against the mean centroid size of each group were computed to evaluate allometry using the ‘geomorph’ v. 3.1.1 R package (Adams et al., 2020) in each sample subset.. All plots were done using the packages ‘ggpubr’ v. 0.4.0. and ‘ggplot2’ v. 3.3.6.

Morphological differences regarding the present/absence of the glenoid *labrum* were tested by performing a Procrustes ANOVA on the 2D and the 3D sample with Bonferroni post-hoc test, using the ‘geomorph’ v. 3.1.1 R package (Adams et al., 2020).

### 2.4. 2D areas

From the zenithal images, we calculated two-dimensional areas (with and without glenoid *labrum*) with ImageJ 1.53e (Schneider, Rasband, & Eliceiri, 2012) and we visualized the group differences through a box-and-whisker plot.

## 3. Results

### 3.1. Geometric morphometrics

#### *Principal Components Analyses*

**3D geometric morphometrics PCAs**. The PCA for the glenoid without *labrum* yields 11 principal components (PCs), of which the first six components explain 89.9% of the total variance (Fig. 2A, SI Fig. 1, 2, 3, 4, and Table 2). We did not consider PCs with <5% variance throughout the analyses as they did not yield any meaningful patterns, but all are reported in Table 2. PC1 is driven by differences in glenoid depth, with individuals with more negative scores having deeper glenoids. Group differences are not clearly established, but are somewhat clearer in PC1, especially for hylobatids, which occupy a different space from the other groups, and *Homo sapiens*, which cluster together in the middle of the scatterplot.

The PCA for the glenoid with *labrum* yields 11 PCs, of which the first six components explain 92.1 % of the total variance (Fig. 2B, SI Fig. 5, 6, 7, 8, and Table 2). PC1 shows differences between *Pan* and *Homo*, yet cercopithecoids overlap with every group (with hylobatids and chimpanzees to a lesser extent). PC1 mainly represents depth variation, whereas PC2 variation is driven by glenoid outline differences, where, in the positive end, scores represent a glenoid with an elongated mid-inferior portion, and, in the negative end, they represent glenoids with an extended mid-superior portion.

**2D geometric morphometrics PCAs**. The PCA for the glenoid without *labrum* yields 12 PCs, of which the first three components explain 83.8 % of the total variance (Fig. 3A, SI Fig. 9, and Table 2). PC1 represent variation between pear-shaped and oval glenoids, in both cases with elongated shape in contrast with PC2, which shows differences between elongated and rounded glenoids, and display a better group separation, although cercopithecoids and *Pan* overlap with the other groups.

The PCA for the glenoid with *labrum* yields 12 PCs, of which the first five components explain 85.2% of the total variance (Fig. 3B, SI Fig. 10, 11, 12, and Table 2). PC1 shows differences between rounded and pear-shaped glenoids, whereas PC2 shows slight differences in elongation.

*Phylogenetic Principal Components Analyses*

**3D geometric morphometrics phy-PCAs**. The phy-PCA for the glenoid without *labrum* yields eight PCs, of which the first four components explain 91.8% of the total variance (Fig. 4A and Table 3). Hominoids cluster together in the middle of the scatterplot, however the cercopithecoids variability is widest and they overlap with every other group. Shape changes are driven by depth in both PC1 and PC2, although less markedly than in the non-phylogenetically adjusted PCA.

The phy-PCA for the glenoid with *labrum* yield eight PCs, of which the first five components explain 94.2 % of the total variance (Fig. 4B and Table 3). *Nomascus* is separated from the other groups, and while PC2 shows differences between *Pan* and *Homo*, cercopithecoids overlap with every group. PC1 shows differences in depth and PC2 shows differences in glenoid outline, with somewhat rounder glenoids on the negative end, and glenoids with an elongated mid-superior portion on the negative end.

**2D geometric morphometrics phy-PCAs**. The phy-PCA for the glenoid without *labrum* yield 12 PCs, of which the first four components explain 93.0 % of the total variance (Fig. 5A and Table 3). Hylobatids fall outside the variability of cercopithecoids, which encompass that of the other hominoids, however, every hylobatid species occupies a different location in the morphospace, not clustering together. PC1 represent variation between pear-shaped and oval glenoids and PC2 differences between elongated and rounded glenoids.

The PCA for the glenoid with *labrum* yields 12 PCs, of which the first five components explain 92.7% of the total variance (Fig. 5B and Table 3). Both PCs represent variation between pear-shaped (positive end) and oval (negative end) glenoids.

*OLS and PGLS regressions*

No PC is significantly correlated with ln CS (for all sample subsets, $p > 0.05$; Table 4), meaning size does not account for shape variation. The PGLS on mean group coordinates and mean centroid size is not significant ($p > 0.05$ for all sample subsets; Table 4). Centroid size explain very little in all 2D subsets and 3D subset without *labrum* ($R^2 < 0.10$), however, for the 3D subset, centroid size explained 13% of the variance without *labrum* in 3D ($R^2 = 0.134$) and 12% of the variance with *labrum* in 3D ($R^2 = 0.121$; Table 4), but did not reach significance ($p = 0.314$ and $p = 0.352$, respectively).

*Procrustes ANOVA*

There is no significant difference between species, regardless of the presence of the *labrum*, in both 2D ($Z = 0.469$; $p = 0.320$) and 3D samples ($Z = 0.194$; $p = 0.440$); however, within the Bonferroni post-hoc using 2D data, some intragroup differences between presence and absence of *labrum* were found for *Cercopithecus ascanius*, *Chlorocebus aethiops*, *Macaca sylvanus*, *Miopthecus ogouensis* for the cercopithecoids, and *Nomascus gabriellae* for hominoids (the full results of the Bonferroni post-hoc can be found the supplementary material SI Table 4, for the 2D sample, and SI Table 5, for the 3D sample).

3.2. 2D areas

The box-and-whisker plot (Fig. 6) shows a trend to an increase in absolute values of glenoid cavity surface area with the presence of *labrum* in all groups, and that the increase is most acute in humans and, to a lesser degree, in chimpanzees.

## 4. Discussion

We have investigated the effects of the glenoid *labrum* in relation to the function and morphology of the glenoid cavity and the overall glenohumeral joint. Overall, the results suggest that the presence of the glenoid *larbum* might change the depth, area, and shape of the contour of the glenoid cavity. We further discuss the results of the 3DGM analyses and surface area availability analyses below.

### 4.1.Geometric morphometrics

Our results indicate that the morphology and variability of dry-bone glenoid cavities are comparable to that reported by previous works of hominoids (Arias-Martorell et al., 2015; Larson, 1998; Larson 2013; Macias & Churchill, 2015; Roberts, 1974). In most studies the skeletonized glenoid cavities of hominoids tend to display an intermediate morphology between oval and round, with hylobatids having the roundest glenoids. Cercopithecoids, on the other hand, are found here to display a great amount of variation, not showing the marked pear-shaped morphology reported in previous works (e.g., Arias-Martorell et al., 2015; Selby, Lovejoy, & Byron, 2020). This is the case of the two *Papio* and the *Cercocebus* individuals, which do not present a pear-shaped glenoid. Instead, they present a single notch on one side of the glenoid cavity, making the overall glenoid contour morphology more hominoid-like—and thus overlapping with apes.

When the *labrum* is present, the morphology of the glenoid cavity differs from its morphology observed in dry-bone material. In the 2D analyses, intragroup variation increases, and group distribution within the morphospace is not as clear-cut as without the presence of the glenoid *labrum* (e.g., Roberts, 1974). The glenoid cavity of chimpanzees without *labrum* displays an intermediate morphology; the presence of the *labrum* changes the morphology of the glenoid to a more elongated structure, due to uneven thickness of the *labrum*, which appears to be thicker at the inferior margin. The resulting morphology of glenoid cavities of chimpanzees with *labrum* is closer to quadrupedal cercopithecoids than to arboreal apes, which could potentially be related to functional demands of the more terrestrial locomotor behavior of chimpanzees (e.g., knuckle-walking). Gorillas, which are in general less arboreal than chimpanzees in adulthood (Hunt, 1991), should be included in the analysis to test this hypothesis in future studies.

In general, the changes in thickness of the *labrum* appears to be particular to each species in the present study; in this regard, thickness varies along the glenoid cavity margin thus changing its morphology. Certainly, there are significant differences in the glenoid cavity morphology with and without *labrum* in four groups of cercopithecoids (*Chlorocebus aethiops, Cercopithecus ascanius, Miopithecus ogouensis*, and *Macaca sylvanus*) and one hominoid (*Nomascus*). The sample size of all our groups is very small, therefore, it is possible that larger samples might lead to more significant differences in thickness and morphology in future studies.

The 3D analyses allow the characterization of glenoid depth and show a clearer group separation than the 2D analyses. The presence of the *labrum* increases the depth of the glenoid and depth increase is the main feature distinguishing hominoids from cercopithecoids. Among hominoids, hylobatids show the most increase in depth. *Cercocebus* (which morphologically resembled hominoids in the 2D analyses), when depth is considered, appears different from *Pan* and *Homo*. That is not the case for *Papio*, whose glenoid depth appears to be more hominoid-like (together with its glenoid contour morphology). Intriguingly, *Papio* is a terrestrial quadruped, therefore, more studies are needed to evaluate whether there are similarities in *Papio* and hominoids regarding forearm use that might account for their resemblance in glenohumeral joint morphology.

In the case of humans, the glenoid *labrum* seems to be increasing the depth of the glenoid cavity. Dry-bone glenoid cavities of humans are already deeper than other apes in our study, but the presence of a thick and large *labrum* considerably contributes to the ball-and-socket nature of the human glenohumeral joint. The head of the humerus moves through the socket structure created by the glenoid cavity and the *labrum* in humans (Howell & Galinat, 1989), therefore, the depth increase afforded by the *labrum* in humans might be indicative of an improvement in the stability of the glenohumeral joint due to a better articular contact between the glenoid cavity and the humeral head. The manipulatory abilities of humans might demand more stability at the glenohumeral joint to aid in fine motor skills and arm repositioning capabilities for hand manipulation—as is the case of humeral torsion, which is related to hand manipulation (Larson, 2013), a greater stability of the glenohumeral joint could also represent additional manipulation-related features of the human arm (Larson, 2013). However, more studies are needed to further assess this possibility.

The phylogenetic relationships between the groups included in this study do not seem to influence the shape of the glenoid cavity with or without *labrum*, thus, the morphological characteristics of the glenoid found here are more probably related to function than to phylogeny. However, larger samples that would enable other, more accurate tests (such as phylogenetic signal analyses) have to be undertaken in the future to further evaluate the influence of phylogeny in glenoid shape with and without *labrum*.

### 4.2. Glenoid cavity surface area availability

The regression between shape and centroid size—a proxy for body mass—even when adjusted for phylogenetic relationships between groups, does not yield significant results. Therefore, body mass does not seem to be influencing the morphological changes in glenoid shape with or without *labrum* either in the 2D or 3D subsets. However, the reported values of the 2D area, depicted in the box-and-whisker plot (which are absolute, not relative), show noticeable body mass differences between groups. As such, more analyses are needed to ascertain the influence of body mass regarding the thickness of the *labrum* in larger species.

Nevertheless, an overall intragroup increase in articular surface area in glenoid cavities with *labrum* in the 2D surface area values can be observed. Humans display the most acute increase in articular surface area of all groups, followed by chimpanzees. Even if related to differences in body mass, the intragroup increase in surface area does not preclude the possibility of a reduced size gap between glenoid cavity and the humeral head for all the species included in the analyses, but particularly so for humans when the *labrum* is present. This might influence the functionality of the glenohumeral joint and could potentially have an impact on the interpretations associated with joint surface availability derived from dry-bone material alone.

Finally, of particular interest are the functional inferences derived from fossil material where the characteristics of the *labrum* cannot be ascertained. For example, the Early Miocene ape *Morotopithecus* is considered to have engaged in suspensory behaviors based on the morphology of its glenoid cavity (MacLatchy et al., 2000). However, in light of the results found here, functional inferences derived from the morphology of dry-bone glenoid cavities might not reflect the functionality of the glenohumeral joint *in vivo*. More studies are needed in order to better characterize the relationship between dry-bone glenoid cavity morphology and the *labrum*, and, in general, to better ascertain the influence of soft tissue in bone and joint function. In the same vein, more sample is needed to confirm the trends found in this study regarding changes in glenoid surface area and morphology.

### 4.3. Limitations

Several limitations have been identified with our study which need to be addressed. The need to work with frozen fresh cadaveric samples to characterize soft tissue morphology is a significant limitation for this study because it severely limits the sample sizes we can accrue per each group due to availability of primates for dissection. This is also an issue for obtaining wide-ranging age and sex representation, and, especially, for acquiring data on both left and right sided glenoid cavities, which could be introducing a bias in species that show some degree of handedness. However, to the best of our knowledge, there are no studies exploring the effects of handedness on forelimb morphology and vice versa, therefore, more studies are needed to understand this potential bias introduced in our study. Another issue identified is the relative lack of locomotor diversity represented in the sample, particularly among cercopithecoids. Introducing groups such as colobines, for example, which show behaviors such as leaping and even suspension (Byron & Covert, 2004), or non-catarrhine monkeys such as atelids, which also show a diversity of locomotor behaviors, some of which convergently with apes (Cant, Youlatos & Rose, 2001) would be a priority in future studies.

In addition, we encountered some limitations with photogrammetry (for a review on the method and its use see, e.g., Fourie, Damstra, Gerrits, & Ren, 2011, and references therein) when used to record soft tissue anatomy: good photogrammetric reconstructions did not depend on number of pictures taken, since we obtained good to medium quality 3D digital surface images with sets of pictures ranging from 17 to 101, as well as some low-quality reconstructions with 100-picture sets (e.g., a *Nomascua gabriellae* individual (NG03); SI Table 1). Other factors that influenced the quality of reconstructions were lighting conditions, keeping a continuous set of overlapping pictures in all axes, and maintaining focal distance, which was not always possible (oftentimes necropsy/dissection labs have limited conditions and space to properly set up equipment). The more homogenous bone tissue resulted in 3D digital surface images of good quality in all instances.

## 5. Conclusions

The glenoid cavity shape changes depending on whether the *labrum* is present, thus some functional inferences (e.g., high mobility in humans) of the glenoid would not be consistent with the functional interpretations of glenoid cavities with the presence of *labrum*. The presence of the glenoid *labrum* increases the depth and area of the glenoid cavity, extending contact with the head of the humerus, thus suggesting that the stability of the glenohumeral joint is improved and its mobility might be more limited than previously anticipated, particularly in humans.

## Acknowledgements

We are grateful to A. Urciuoli for their help with the analyses. This work is part of R+D+I project PID2020-116908GB-I00, funded by the *Agencia Estatal de Investigación* of the Spanish Ministry of Science and Innovation (MCIN/AEI/10.13039/501100011033/). It is also funded by MCIN and the European

Union (FSE+) through *Ayudas para Contratos Predoctorales para la Formación de Doctores* (FPI) of the Agencia Estatal de Investigación; the Generalitat de Catalunya (AGAUR BP-H2020 MSCA-Cofund No. 801370 to JAM), the Spanish Ministry of Economy and Competitivity of Spain (MINECO) and the EU (FEDER) (CGL2014-52611-C2-2-P to JMP), and the University of Barcelona (APIF-UB 2016/2017 to AC).

## Data availability statement

The data that support the findings of this study are openly available in Zenodo (Zenodo.org) at http://doi.org/10.5281/zenodo.7569015.

## References

Adams, D., Collyer, M., Kaliontzopoulou, A., & Sherratt, E. (2020). Geomorph: geometric morphometric analyses of 2D/3D landmark data. R package version 3.2, 1.

Arias-Martorell, J. (2019). The morphology and evolutionary history of the glenohumeral joint of hominoids: A review. *Ecology and Evolution*, 9, 703-722. https://doi.org/10.1002/ece3.4392

Arias-Martorell, J., Potau, J. M., Bello-Hellegouarch, G., & Pérez-Pérez, A. (2015a). Like Father, Like Son: Assessment of the Morphological Affinities of A.L. 288–1 (*A. afarensis*), Sts 7 (*A. africanus*) and Omo 119–73–2718 (*Australopithecus sp.*) through a three-dimensional shape analysis of the shoulder joint. *PLoS ONE*, 10, e0117408.

Arnold, C., Matthews, L. J., & Nunn, C. L. (2010). The 10kTrees website: a new online resource for primate phylogeny. *Evolutionary Anthropology*, 19, 114-

118. https://doi.org/10.1002/evan.20251

Ashton, E. H., & Oxnard, C. E. (1964). Functional adaptations in the primate shoulder girdle. *Proceedings of the Zoological Society of London*, 142, 49-66. https://doi.org/10.1111/j.1469-7998.1964.tb05153.x

Beltran, J., Rosenberg, Z. S., Chandnani, V. P., Cuomo, F., Beltran, S., & Rokito, A. (1997). Glenohumeral instability: evaluation with MR arthrography. *RadioGraphics*, 17, 657-673. https://doi.org/10.1148/radiographics.17.3.9153704

Byron, C. D. & Covert, H. H. (2004). Unexpected locomotor behaviour: brachiation by an Old World monkey (*Pygathrix nemaeus*) from Vietnam. *Journal of Zoology*, 263, 101-106. https://doi:10.1017/S0952836904004935

Cant, J. G., Youlatos, D., & Rose, M. D. (2001). Locomotor behavior of *Lagothrix lagothricha* and *Ateles belzebuth* in Yasuni National Park, Equador: general patterns and nonsuspensory modes. *Journal of Human Evolution*, 41, 141-166. https://doi.org/10.1006/jhev.2001.0485

Chan, L. K. (2007). Glenohumeral mobility in primates. *Folia Primatologica*, 78, 1-18. https://doi.org/10.1159/000095682

Chan, L. K. (2008). The range of passive arm circumduction in primates: do hominoids really have more mobile shoulders? *American Journal of Physical Anthropology*, 136, 265-277. https://doi.org/10.1002/ajpa.20800

Corruccini, R. S., & Ciochon, R. L. (1978). Morphoclinal variation in the anthropoid shoulder. *American Journal of Physical Anthropology*, 48, 539-542. https://doi.org/10.1002/ajpa.1330480415

Fourie, Z., Damstra, J., Gerrits, P. O., & Ren, Y. (2011). Evaluation of anthropometric accuracy and reliability using different three-dimensional scanning systems. *Forensic science international*, 207, 127-134. https://doi.org/10.1016/j.forsciint.2010.09.018

Godfrey, L., Sutherland, M., Boy, D., & Gomberg, N. (1991). Scaling of limb joint surface areas in anthropoid primates and other mammals. *Journal of Zoology*, 223, 603-625. https://doi.org/10.1016/0047-2484(89)90067-5

Hopkins, W. D., Wesley, M. J., Izard, M. K., Hook, M., & Schapiro, S. J. (2004). Chimpanzees (*Pan troglodytes*) are predominantly right-handed: replication in three populations of apes. *Behavioral Neuroscience*, 118, 659. https://doi.org/10.1037/0735-7044.118.3.659

Howell, S. M., & Galinat, B. J. (1989). The glenoid–labral socket: A constrained articular surface. *Clinical Orthopaedics and Related Research*, 243, 122-125. https://doi.org/10.1097/00003086-198906000-00018

Hunt, K. D. (1991). Positional behavior in the Hominoidea. *International Journal of Primatology*, 12, 95-118. https://doi.org/10.1007/BF02547576

Isler, K. (2005). 3D-kinematics of vertical climbing in hominoids. *American Journal of Physical Anthropology*, 126, 66-81. https://doi.org/10.1002/ajpa.10419

Jungers, W. L. (1991). Scaling of postcranial joint size in hominoid primates. *Human Evolution*, 6, 391-399. https://doi.org/10.1007/BF02435532

Katz, D., & Friess, M. (2014). 3D from standard digital photography of human crania—a preliminary assessment. *American Journal of Physical Anthropology*, 154, 152-158. https://doi.org/10.1002/ajpa.22468

Klingenberg, C. P. (2011). MorphoJ: an integrated software package for geometric morphometrics. *Molecular ecology resources*, 11, 353-357. https://doi.org/10.1111/j.1755-0998.2010.02924.x

Lague, M. R., & Jungers, W. L. (1999). Patterns of sexual dimorphism in the hominoid distal humerus. *Journal of Human Evolution*, 36, 379-399. https://doi.org/10.1006/jhev.1998.0274

Larson, S. G., & Stern Jr, J. T. (1986). EMG of scapulohumeral muscles in the chimpanzee during reaching and "arboreal" locomotion. *American Journal of Anatomy*, 176, 171-190. https://doi.org/10.1002/aja.1001760207

Larson, S. G. (1988). Subscapularis function in gibbons and chimpanzees: implications for interpretation of humeral head torsion in hominoids. *American Journal of Physical Anthropology*, 76, 449-462. https://doi.org/10.1002/ajpa.1330760405Larson, S. G. (1995). New characters for the functional interpretation of primate scapulae and proximal humeri. *American Journal of Physical Anthropology*, 98, 13-35. https://doi.org/10.1002/ajpa.1330980103

Larson, S.G. (2013). Shoulder Morphology in Early Hominin Evolution. In Reed, K., Fleagle, J., Leakey, R. (Eds), *The Paleobiology of Australopithecus. Vertebrate Paleobiology and Paleoanthropology* (pp. 247–261). Springer. https://doi.org/10.1007/978-94-007-5919-0_17Macias, M. E., & Churchill, S. E. (2015). Functional morphology of the Neandertal scapular glenoid fossa. *The Anatomical Record*, 298, 168-179. https://doi.org/10.1002/ar.23072

MaClatchy, L., Gebo, D., Kityo, R., & Pilbeam, D. (2000). Postcranial functional morphology of *Morotopithecus bishopi*, with implications for the evolution of modern ape locomotion. *Journal of Human Evolution*, 39, 159-183. http://doi.org/10.1006/jhev.2000.0407

Margiotoudi, K., Marie, D., Claidière, N., Coulon, O., Roth, M., Nazarian, B., Lacoste, R., Hopkins, W. D., Molesti, S. & Meguerditchian, A. (2019). Handedness in monkeys reflects hemispheric specialization within the central sulcus. An in vivo MRI study in right-and left-handed olive baboons. *Cortex*, 118, 203-211. https://doi.org/10.1016/j.cortex.2019.01.001

Morino, L., Uchikoshi, M., Bercovitch, F., Hopkins, W. D., & Matsuzawa, T. (2017). Tube task hand preference in captive hylobatids. *Primates*, 58, 403-412. https://doi.org/10.1007/s10329-017-0605-z

Preuschoft, H., Hohn, B., Scherf, H., Schmidt, M., Krause, C., & Witzel, U. (2010). Functional Analysis of the Primate Shoulder. *International Journal of Primatology*, 31, 301–320. https://doi.org/10.1007/s10764-010-9399-1

Roberts, D. (1974). Structure and function of the primate scapula. In Jenkins, F. A. (Ed), *Primate locomotion* (pp. 171-200). Academic Press.

Rohlf, F. J. (2015). The tps series of software. *Hystrix*, 26, 9-12. https://doi.org/10.4404/hystrix-26.1-11264

Rose, M. D. (1989). New postcranial specimens of catarrhines from the Middle Miocene Chinji Formation, Pakistan: descriptions and a discussion of proximal humeral functional morphology in anthropoids. *Journal of Human Evolution*, 18, 131-162. http://doi.org/10.1111/j.1469-7998.1991.tb04391.x

Schlager, S. (2017). Morpho and Rvcg–shape analysis in R: R-packages for geometric morphometrics, shape analysis and surface manipulations. *Statistical shape and deformation analysis* (pp. 217-256). Elsevier. https://doi.org/10.1016/B978-0-12-810493-4.00011-0

Schneider, C. A., Rasband, W. S., & Eliceiri, K. W. (2012). NIH Image to ImageJ: 25 years of image analysis. *Nature methods*, 9, 671-675. https://doi.org/10.1038/nmeth.2089

Selby, M. S., Lovejoy, C. O., & Byron, C. D. (2020). Odd-nosed monkey scapular morphology converges on that of arm-swinging apes. *Journal of Human Evolution*, 143, 102784. https://doi.org/10.1016/j.jhevol.2020.102784

Wiley, D. F., Amenta, N., Alcantara, D. A., Ghosh, D., Kil, Y. J., Delson, E., Harcourt-Smith, W., Rohlf, F. J., St John, K., & Hamann, B. (2005). *Evolutionary morphing* (pp. 431-438). IEEE. https://doi.org/10.1109/VISUAL.2005.1532826.

Young, N. M. (2008). A comparison of the ontogeny of shape variation in the anthropoid scapula: functional and phylogenetic signal. *American Journal of Physical Anthropology*, 136, 247-264. https://doi.org/10.1002/ajpa.20799

## Figure Legends

**Figure 1.** Landmark configurations (protocols) of the glenoid cavity of the scapula used in the 3D geometric morphometric analysis with *labrum* (A) and without *labrum* (B), and in the 2D geometric morphometrics analysis with *labrum* (C) and without *labrum* (D) shown in a human glenoid (in frontal view).

**Figure 2.** PC1 vs PC2 plot derived from 3D landmarks collected on glenoid cavities without *labrum* (A) and with *labrum* (B). Deformation grids represent the shape of the outline of the glenoid cavity in anterior (frontal), and side view, superior to inferior oriented. Taxon abbreviations: Hs, *Homo sapiens*; Pt, *Pan troglodytes*; Hl, *Hylobates lar*; Ng, *Nomascus gabriellae*; Ph, *Papio hamadryas*; Ca, *Chlorocebus aethiops*; Cal, *Cercocebus atys lunulatus*; Mo, *Miopithecus ogouensis*; Cas, *Cercopithecus ascanius.*

**Figure 3.** PC1 vs PC2 plot derived from 2D landmarks collected on glenoid cavities without *labrum* (A) and with *labrum* (B). Deformation grids represent the shape of the outline of the glenoid cavity in anterior (frontal), and side view, superior to inferior oriented. Taxon abbreviations: Hs, *Homo sapiens*; Pt, *Pan troglodytes*; Hl, *Hylobates lar*; Ng, *Nomascus gabriellae*; Ssy, *Symphalangus syndactylus*; Ph, *Papio hamadryas*; Mto, *Macaca tonkeana*; Msi, *Macaca silenus*; Msy, *Macaca sylvanus*; Ca, *Chlorocebus aethiops*; Cal, *Cercocebus atys lunulatus*; Mo, *Miopithecus ogouensis*; Cas, *Cercopithecus ascanius.*

**Figure 4.** Phylogenetic (phy-)PC1 vs phy-PC2 plot derived from 3D landmarks collected on glenoid cavities without *labrum* (A) and with *labrum* (B). Deformation grids represent the shape of the outline of the glenoid cavity in anterior (frontal), and side view, superior to inferior oriented. Taxon abbreviations: Hs, *Homo sapiens*; Pt, *Pan troglodytes*; Hl, *Hylobates lar*; Ng, *Nomascus gabriellae*; Ph, *Papio hamadryas*; Ca, *Chlorocebus aethiops*; Cal, *Cercocebus atys lunulatus*; Mo, *Miopithecus ogouensis*; Cas, *Cercopithecus ascanius.*

**Figure 5.** Phylogentic (phy-)PC1 vs phy-PC2 plot derived from 2D landmarks collected on glenoid cavities without *labrum* (A) and with *labrum* (B). Deformation grids represent the shape of the outline of the glenoid cavity in anterior (frontal), and side view, superior to inferior oriented. Taxon abbreviations: Hs, *Homo sapiens*; Pt, *Pan troglodytes*; Hl, *Hylobates lar*; Ng, *Nomascus gabriellae*; Ssy, *Symphalangus syndactylus*; Ph, *Papio hamadryas*; Mto, *Macaca tonkeana*; Msi, *Macaca silenus*; Msy, *Macaca sylvanus*; Ca, *Chlorocebus aethiops*; Cal, *Cercocebus atys lunulatus*; Mo, *Miopithecus ogouensis*; Cas, *Cercopithecus*

*ascanius*.

**Figure 6.** Box-and-whisker plot of 2D areas (cm$^2$) of the glenoid cavity with (L) and without (NoL) the glenoid labrum. Group abbreviation: Ce, cercopithecoids; Hy, hylobatids; Pt, *Pan troglodytes*; Hs, *Homo sapiens*.

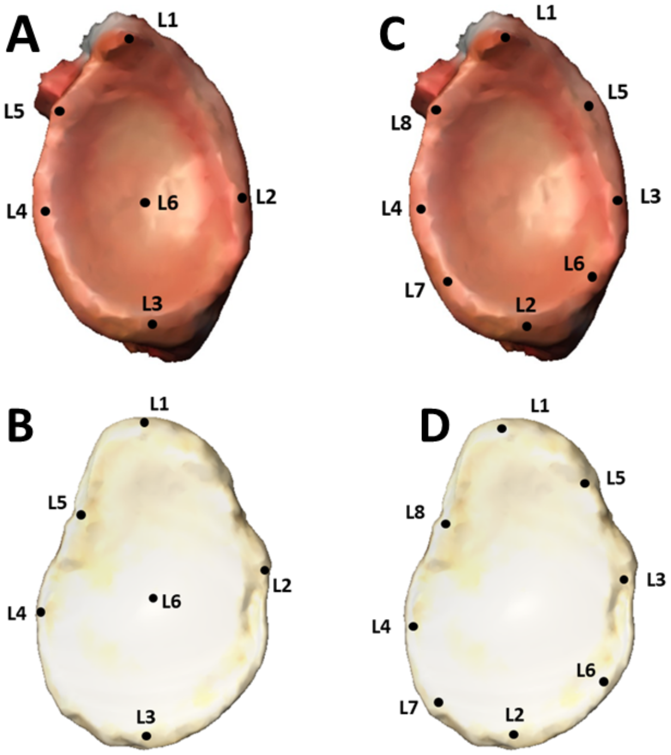
A
L1
L5
L4
L6
L2
L3
C
L1
L5
L8
L4
L3
L6
L7
L2
B
L1
L5
L2
L6
L4
L3
D
L1
L5
L8
L3
L4
L6
L7
L2

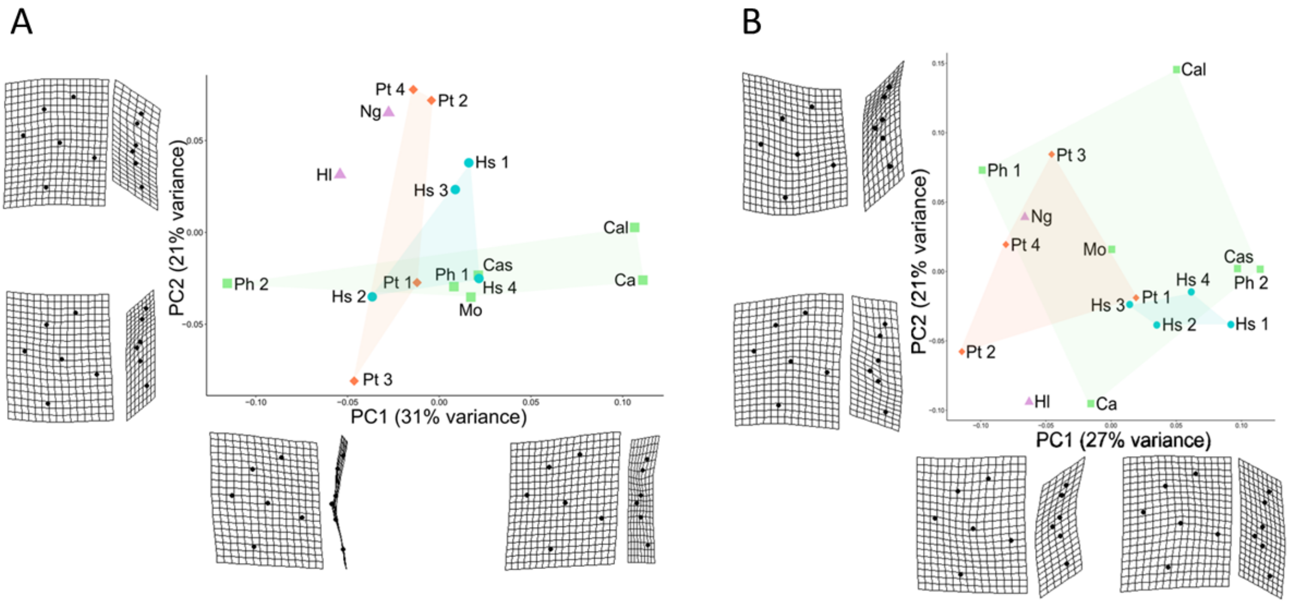
A
PC1 (31% variance)
PC2 (21% variance)
-0.10
-0.05
0.00
0.05
0.10
0.05
0.00
-0.05
Pt 4
Pt 2
Ng
Hs 1
Hl
Hs 3
Cal
Ph 2
Ph 1
Cas
Hs 2
Pt 1
Hs 4
Ca
Mo
Pt 3
B
PC1 (27% variance)
PC2 (21% variance)
0.15
0.10
0.05
0.00
-0.05
-0.10
-0.10
-0.05
0.00
0.05
0.10
Cal
Pt 3
Ph 1
Ng
Pt 4
Mo
Cas
Ph 2
Hs 4
Pt 1
Hs 3
Hs 2
Hs 1
Pt 2
Hl
Ca

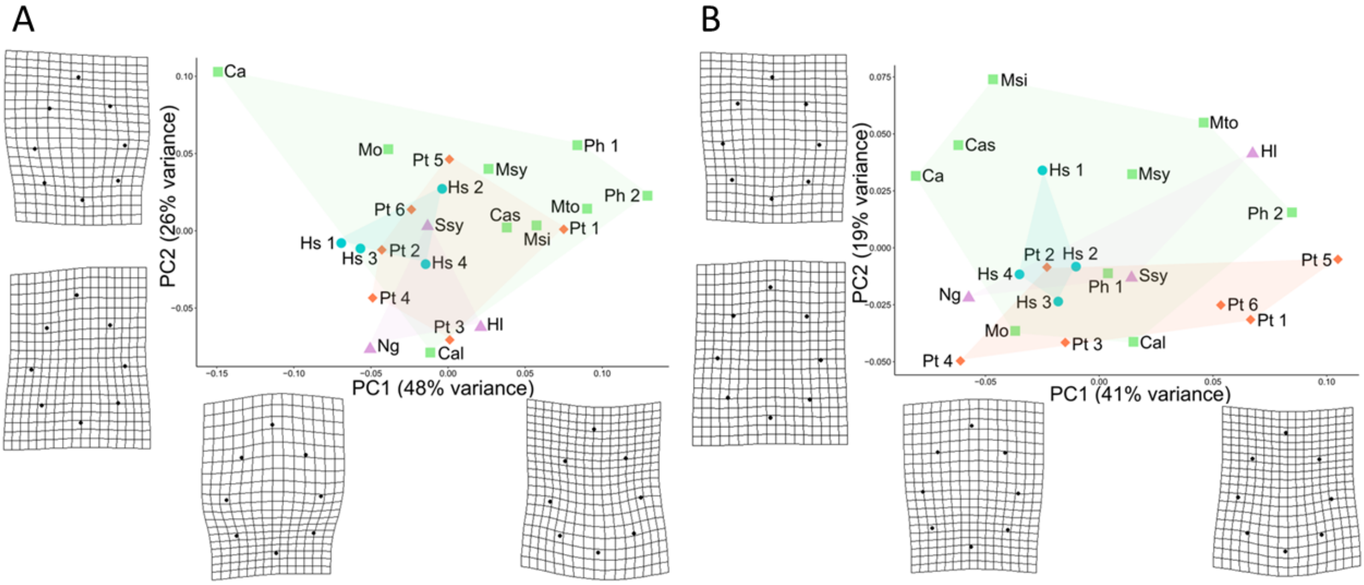
A
PC1 (48% variance)
PC2 (26% variance)
-0.15
-0.10
-0.05
0.00
0.05
0.10
Ca
Mo
Pt 5
Msy
Hs 2
Ph 1
Ph 2
Pt 6
Mto
Cas
Ssy
Msi
Pt 1
Hs 1
Hs 3
Pt 2
Hs 4
Pt 4
Pt 3
Hl
Ng
Cal
B
PC1 (41% variance)
PC2 (19% variance)
0.075
0.050
0.025
0.000
-0.025
-0.050
-0.05
0.00
0.05
0.10
Msi
Mto
Cas
Hl
Hs 1
Msy
Ca
Ph 2
Pt 2
Hs 2
Pt 5
Hs 4
Ph 1
Ssy
Ng
Hs 3
Pt 6
Pt 1
Mo
Pt 3
Cal
Pt 4

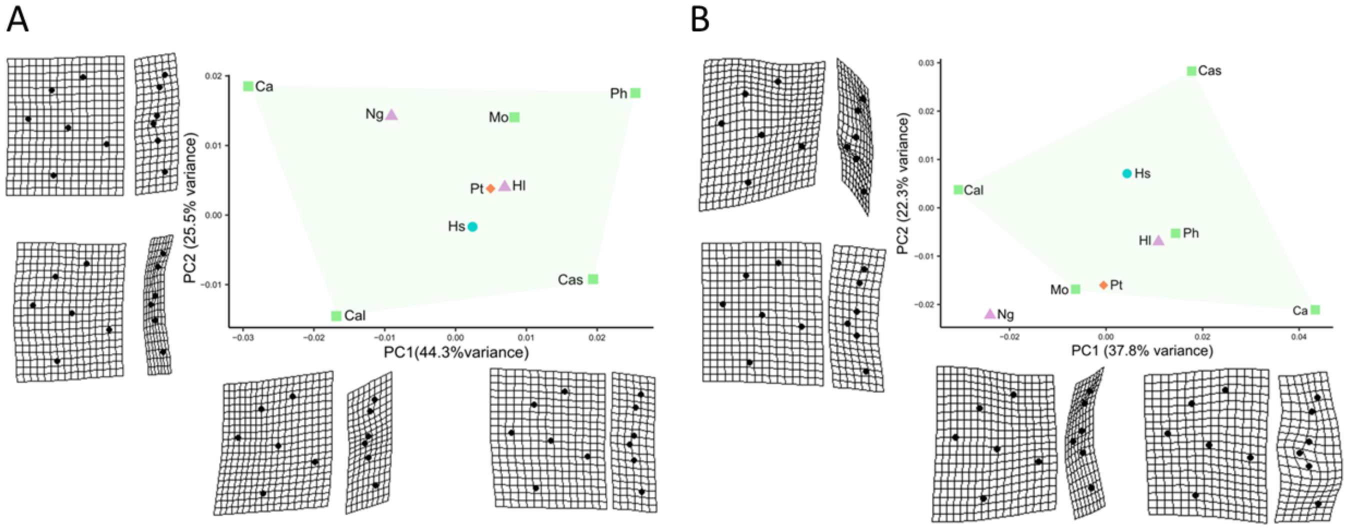
A
Ca
Ng
Mo
Ph
Pt
Hl
Hs
Cas
Cal
PC2 (25.5% variance)
PC1(44.3%variance)
0.02
0.01
0.00
-0.01
-0.03
-0.02
-0.01
0.00
0.01
0.02
B
Cas
Hs
Cal
Ph
Hl
Mo
Pt
Ng
Ca
PC2 (22.3% variance)
PC1 (37.8% variance)
0.03
0.02
0.01
0.00
-0.01
-0.02
-0.02
0.00
0.02
0.04

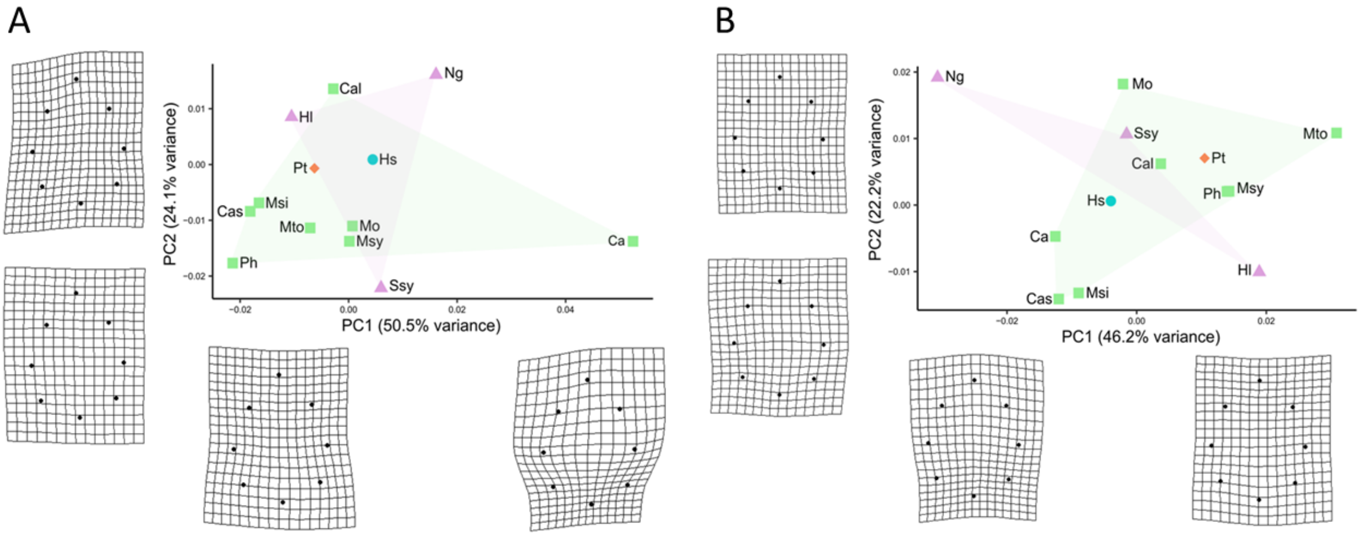
A
PC2 (24.1% variance)
0.01
0.00
−0.01
−0.02
−0.02
0.00
0.02
0.04
PC1 (50.5% variance)
Ng
Cal
Hl
Hs
Pt
Cas
Msi
Mto
Mo
Msy
Ca
Ph
Ssy
B
PC2 (22.2% variance)
0.02
0.01
0.00
−0.01
−0.02
0.00
0.02
PC1 (46.2% variance)
Ng
Mo
Ssy
Mto
Cal
Pt
Ph
Msy
Hs
Ca
Hl
Cas
Msi

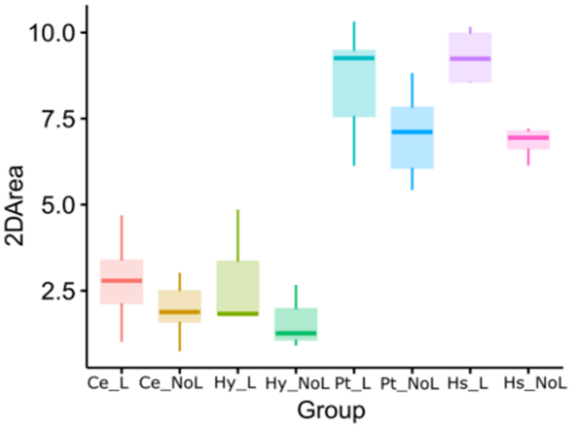
10.0
7.5
5.0
2.5
2DArea
Ce_L
Ce_NoL
Hy_L
Hy_NoL
Pt_L
Pt_NoL
Hs_L
Hs_NoL
Group

**Table 1.** Details of the comparative sample (N =22), including sample size (N), number of specimens per side (Lat), and institution.

| Group | Specie | N | Lat | | Institution |
|---|---|---|---|---|---|
| | | | R | L | |
| Cercopihtecines | *Chlorocebus aetiops* | 1 | - | 1 | AMUV† |
| | *Cercocebus atys lunulatus* | 1 | 1 | - | AMUV |
| | *Cercopithecus ascanius* | 1 | 1 | - | AMUV |
| | *Miopithecus ogoensis* | 1 | - | 1 | AMUV |
| | *Macaca silenus* | 1 | 1 | - | AMUV |
| | *Macaca sylvanus* | 1 | - | 1 | AMUV |
| | *Macaca tonkeana* | 1 | 1 | - | AMUV |
| | *Papio hamadryas* | 2 | 1 | 1 | AMUV |
| Hylobatids | *Symphalangus syndactylus* | 1 | 1 | - | AMUV |
| | *Hylobates lar* | 1 | - | 1 | AMUV |
| | *Nomascus gabriellae* | 1 | - | 1 | AMUV |
| *Pan troglodytes* | *Pan troglodytes* | 6 | 3 | 3 | AMUV |
| *Homo sapiens* | *Homo sapiens* | 4 | - | 4 | BDSUB† |

† Abbreviations: AMUV, Anatomical Museum of the University of Valladolid; BDSUB, Body Donation Service of the Faculty of Medicine of the University of Barcelona; L, left; R, right

**Table 2.** Results for the Principal Component Analyses (PCA) with the eigenvalues (Eigenval), the variance (% Var) and the cumulative variance (% Cumul) for each Principal Component (PCs) recovered in the analyses.

| | 3D without *labrum* | | | 3D with *labrum* | | | 2D without *labrum* | | | 2D with *labrum* | | |
|---|---|---|---|---|---|---|---|---|---|---|---|---|
| PCs | Eigenval | % Var | % Cumul | Eigenval | % Var | % Cumul | Eigenval | % Var | Cumul % | Eigenval | % Var | % Cumul |
| PC1 | 0.00450832 | 36.515 | 36.515 | 0.00515790 | 26.840 | 26.840 | 0.00388594 | 48.015 | 48.015 | 0.00267182 | 41.403 | 41.403 |
| PC2 | 0.00265666 | 21.517 | 58.032 | 0.00396391 | 20.627 | 47.467 | 0.00213534 | 26.385 | 74.400 | 0.00123629 | 19.158 | 60.560 |
| PC3 | 0.00151109 | 12.239 | 70.271 | 0.00369729 | 19.240 | 66.707 | 0.00075309 | 9.305 | 83.705 | 0.00059673 | 9.247 | 69.807 |
| PC4 | 0.00128778 | 10.430 | 80.701 | 0.00239042 | 12.439 | 79.146 | 0.00040343 | 4.985 | 88.690 | 0.00056658 | 8.780 | 78.587 |
| PC5 | 0.00076631 | 6.207 | 86.908 | 0.00141054 | 7.340 | 86.486 | 0.00022726 | 2.808 | 91.498 | 0.00042669 | 6.612 | 85.199 |
| PC6 | 0.00061933 | 5.016 | 91.924 | 0.00107009 | 5.568 | 92.054 | 0.00020725 | 2.561 | 94.059 | 0.00030463 | 4.721 | 89.920 |
| PC7 | 0.00042585 | 3.449 | 95.373 | 0.00062008 | 3.227 | 95.281 | 0.00016803 | 2.076 | 96.135 | 0.00024634 | 3.817 | 93.737 |
| PC8 | 0.00028321 | 2.294 | 97.667 | 0.00041075 | 2.137 | 97.418 | 0.00012716 | 1.571 | 97.706 | 0.00017496 | 2.711 | 96.448 |
| PC9 | 0.00017068 | 1.382 | 99.050 | 0.00025413 | 1.322 | 98.741 | 0.00009387 | 1.160 | 98.866 | 0.00008566 | 1.327 | 97.776 |
| PC10 | 0.00007727 | 0.626 | 99.675 | 0.00015032 | 0.782 | 99.523 | 0.00005088 | 0.629 | 99.495 | 0.00006774 | 1.050 | 98.825 |
| PC11 | 0.00004007 | 0.325 | 100.000 | 0.00009168 | 0.477 | 100.000 | 0.00003306 | 0.408 | 99.903 | 0.00004590 | 0.711 | 99.537 |
| PC12 | - | - | - | - | - | - | 0.00000783 | 0.097 | 100.000 | 0.00002990 | 0.463 | 100.000 |

**Table 3.** Results for the Phylogenetic Principal Component Analyses with the eigenvalues (Eigenval), the variance (% Var) and the cumulative variance (% Cumul) for each Principal Component (PCs) recovered in the analyses.

| | 3D without *labrum* | | | 3D with *labrum* | | | 2D without *labrum* | | | 2D with *labrum* | | |
|---|---|---|---|---|---|---|---|---|---|---|---|---|
| | Eigenval | % Val | % Cumul | Eigenval | % Val | % Cumul | Eigenval | % Val | % Cumul | Eigenval | % Val | % Cumul |
| PC1 | 0.00029892 | 44.280 | 44.280 | 0.00051141 | 37.753 | 37.753 | 0.00036085 | 50.502 | 50.502 | 0.00026481 | 46.186 | 46.186 |
| PC2 | 0.00017242 | 25.542 | 69.822 | 0.00030232 | 22.317 | 60.070 | 0.00017239 | 24.126 | 74.628 | 0.00012705 | 22.160 | 68.346 |
| PC3 | 0.00008624 | 12.775 | 82.598 | 0.00020725 | 15.299 | 75.369 | 0.00007686 | 10.757 | 85.385 | 0.00005843 | 10.192 | 78.537 |
| PC4 | 0.00006231 | 9.231 | 91.829 | 0.00014221 | 10.498 | 85.867 | 0.00005455 | 7.634 | 93.019 | 0.00004342 | 7.574 | 86.111 |
| PC5 | 0.00002306 | 3.416 | 95.245 | 0.00011253 | 8.307 | 94.174 | 0.00001825 | 2.555 | 95.574 | 0.00003764 | 6.565 | 92.675 |
| PC6 | 0.00002022 | 2.996 | 98.241 | 0.00006044 | 4.462 | 98.636 | 0.00001634 | 2.286 | 97.860 | 0.00001885 | 3.288 | 95.963 |
| PC7 | 0.00000960 | 1.422 | 99.663 | 0.00001574 | 1.162 | 99.798 | 0.00000924 | 1.293 | 99.154 | 0.00001152 | 2.010 | 97.973 |
| PC8 | 0.00000228 | 0.337 | 100.000 | 0.00000274 | 0.202 | 100.000 | 0.00000323 | 0.452 | 99.605 | 0.00000690 | 1.203 | 99.175 |
| PC9 | - | - | - | - | - | - | 0.00000155 | 0.217 | 99.822 | 0.00000300 | 0.523 | 99.699 |
| PC10 | - | - | - | - | - | - | 0.00000083 | 0.116 | 99.938 | 0.00000114 | 0.199 | 99.898 |
| PC11 | - | - | - | - | - | - | 0.00000044 | 0.061 | 100.000 | 0.00000052 | 0.090 | 99.988 |
| PC12 | - | - | - | - | - | - | 0.00000000 | 0.000 | 100.000 | 0.00000007 | 0.012 | 100.000 |

**Table 4.** Results of the ordinary least-squares (OLS) regression of PC scores (PC1 and PC2) vs. log-transformed centroid size (ln CS), and phylogenetic generalized least-squares (PGLS) of species mean Procrustes coordinates (Pcoords) against the mean centroid size of each group.

| | OLS | | | | | | | | | | | |
|---|---|---|---|---|---|---|---|---|---|---|---|---|
| | 2D without *labrum* | | | 2D with *labrum* | | | 3D without *labrum* | | | 3D with *labrum* | | |
| | $R^2$ | Adjusted $R^2$ | p-value | $R^2$ | Adjusted $R^2$ | p-value | $R^2$ | Adjusted $R^2$ | p-value | $R^2$ | Adjusted $R^2$ | p-value |
| PC1 | 0.001 | -0.049 | 0.885 | 0.029 | -0.019 | 0.448 | 0.009 | -0.061 | 0.717 | 0.101 | 0.036 | 0.231 |
| PC2 | 0.001 | -0.049 | 0.894 | 0.100 | 0.055 | 0.151 | 0.000 | -0.071 | 0.943 | 0.002 | -0.069 | 0.880 |
| | PGLS | | | | | | | | | | | |
| Pccords | 0.02996 | - | 0.766 | 0.01521 | - | 0.923 | 0.134 | - | 0.314 | 0.121 | - | 0.352 |

# Supporting Information

## The morphofunctional implications of glenoid *labrum* of the glenohumeral joint in hominoids

Georgina Raventós-Izard, Josep Mª Potau, Aroa Casado, Juan F Pastor, Julia Arias-Martorell

## Tables

**SI Table 1**. Details of the comparative sample (N=22), including group, specimen ID, side, number of pictures taken with and without the *labrum*, and institution. Abbreviations: AMUV, Anatomical Museum of the University of Valladolid; BDSUB, Body Donation Service of the Faculty of Medicine of the University of Barcelona; L, left; R, right.

| Group | Taxon | ID | Side | N pictures w/ *labrum* | N pictures w/o *labrum* | Institution |
|---|---|---|---|---|---|---|
| Cercopihtecines | *Chlorocebus aetiops* | CA02 | L | 29 | 40 | AMUV |
| | *Cercocebus atys lunulatus* | CAL01 | R | 32 | 53 | AMUV |
| | *Cercopithecus ascanius* | CAS01 | R | 36 | 49 | AMUV |
| | *Miopithecus ogoensis* | MO01 | L | 20 | 50 | AMUV |
| | *Macaca silenus* | MSi03 | R | 21 | 53 | AMUV |
| | *Macaca sylvanus* | MSY01 | L | 17 | 37 | AMUV |
| | *Macaca tonkeana* | MTO01 | R | 41 | 52 | AMUV |
| | *Papio hamadryas* | PH01 | L | 32 | 34 | AMUV |
| | *Papio hamadryas* | PH03 | R | 32 | 47 | AMUV |
| Hylobatids | *Symphalangus syndactylus* | SSy01 | R | 29 | NE † | AMUV |
| | *Hylobates lar* | HL01 | L | 34 | NE † | AMUV |
| | *Nomascus gabriellae* | NG03 | L | 100 | 101 | AMUV |
| Pan troglodytes | *P. troglodytes* | PT05 | L | 31 | 47 | AMUV |
| | *P. troglodytes* | PT06 | R | 24 | 60 | AMUV |
| | *P. troglodytes* | PT07 | R | 36 | 53 | AMUV |
| | *P. troglodytes* | PT08 | R | 27 | 49 | AMUV |
| | *P. troglodytes* | PT09 | L | 34 | 40 | AMUV |
| | *P. troglodytes* | PT10 | L | 24 | 38 | AMUV |
| Homo sapiens | *H. sapiens* | HS051 | L | 96 | 41 | BDSUB |
| | *H. sapiens* | HS052 | L | 74 | 29 | BDSUB |
| | *H. sapiens* | HS053 | L | 79 | 43 | BDSUB |
| | *H. sapiens* | HS055 | L | 48 | 23 | BDSUB |

† Scanning done with next engine laser scanner.

**SI Table 2**. Details of the subset of the sample (N total=16) for the 3D geometric morphometric analyses, including group, species, species sample size (N), number of specimens per side, and institution. Abbreviations: AMUV, Anatomical Museum of the University of Valladolid; BDSUB, Body Donation Service of the Faculty of Medicine of the University of Barcelona; L, left; R, right.

| Group | Species | N | Side | | Institution |
|---|---|---|---|---|---|
| | | | R | L | |
| Cercopihtecines | *Chlorocebus aetiops* | 1 | - | 1 | AMUV |
| | *Cercocebus atys lunulatus* | 1 | 1 | - | AMUV |
| | *Cercopithecus ascanius* | 1 | 1 | - | AMUV |
| | *Miopithecus ogoensis* | 1 | - | 1 | AMUV |
| | *Papio hamadryas* | 2 | 1 | 1 | AMUV |
| Hylobatids | *Hylobates lar* | 1 | - | 1 | AMUV |
| | *Nomascus gabriellae* | 1 | - | 1 | AMUV |
| *Pan troglodytes* | *P. troglodytes* | 4 | 3 | 1 | AMUV |
| *Homo sapiens* | *H. sapiens* | 4 | - | 4 | BDSUB |

**SI Table 3**. Landmark protocols applied for the 2D geometric morphometric and for the 3D geometric morphometric analyses indicating type of landmark and landmark description.

| 2D Landmark Protocol | | | 3D Landmark Protocol | | |
|---|---|---|---|---|---|
| Landmark | Type | Description | Landmark | Type | Description |
| L1 | II | The most superior point of the glenoid contour | L1 | II | The most superior point of the glenoid |
| L2 | II | The most inferior point of the glenoid contour | L2 | II | The most posterior point of the glenoid |
| L3 | II | The most posterior point of the glenoid contour | L3 | II | The most inferior point of the glenoid |
| L4 | II | The most anterior point of the glenoid contour | L4 | II | The most anterior point of the glenoid |
| L5 | III | Middle point between L1 and L3 | L5 | III | Middle point between L1 and L4 |
| L6 | III | Middle point between L2 and L3 | L6 | II | Deepest point of the glenoid |
| L7 | III | Middle pont between L2 and L4 | - | - | - |
| L8 | III | Middle point between L1 and L4 | - | - | - |

**SI Table 4.** Results of the Bonferroni post-hoc with (L) and without (NoL) *labrum* in the 2D sample. Taxon abbreviations: Hs, *Homo sapiens*; Pt, *Pan troglodytes*; Hl, *Hylobates lar*; Ng, *Nomascus gabriellae*; Ssy, *Symphalangus syndactylus*; Ph, *Papio hamadryas*; Mto, *Macaca tonkeana*; Msi, *Macaca silenus*; Msy, *Macaca sylvanus*; Ca, *Chlorocebus aethiops*; Cal, *Cercocebus atys lunulatus*; Mo, *Miopithecus ogouensis*; Cas, *Cercopithecus ascanius*.

| | | Cal | | Cas | | Ca | | Hs | | Hl | | Msi | | Msy | | Mto | | Mo | | Ng | | Pt | | Ph | | Ssy |
|---|---|---|---|---|---|---|---|---|---|---|---|---|---|---|---|---|---|---|---|---|---|---|---|---|---|---|
| | | L | NoL | L | NoL | L | NoL | L | NoL | L | NoL | L | NoL | L | NoL | L | NoL | L | NoL | L | NoL | L | NoL | L | NoL | L |
| Cal | NoL | 1.000 | | | | | | | | | | | | | | | | | | | | | | | | |
| Cas | L | 1.000 | 1.000 | | | | | | | | | | | | | | | | | | | | | | | |
| | NoL | 1.000 | <0.01* | <0.01* | | | | | | | | | | | | | | | | | | | | | | |
| Ca | L | 1.000 | 1.000 | 1.000 | <0.01* | | | | | | | | | | | | | | | | | | | | | |
| | NoL | 1.000 | <0.01* | <0.01* | 1.000 | <0.01* | | | | | | | | | | | | | | | | | | | | |
| Hs | L | 1.000 | 1.000 | 1.000 | 0.202 | 1.000 | 0.148 | | | | | | | | | | | | | | | | | | | |
| | NoL | 1.000 | 1.000 | 1.000 | 1.000 | 1.000 | 0.610 | 1.000 | | | | | | | | | | | | | | | | | | |
| Hl | L | 1.000 | 1.000 | 1.000 | 1.000 | 1.000 | 1.000 | 1.000 | 1.000 | | | | | | | | | | | | | | | | | |
| | NoL | 0.730 | 1.000 | 1.000 | <0.01* | 1.000 | <0.01* | 1.000 | 1.000 | 0.469 | | | | | | | | | | | | | | | | |
| Msi | L | 1.000 | 1.000 | 1.000 | 1.000 | 1.000 | 1.000 | 1.000 | 1.000 | 1.000 | 0.632 | | | | | | | | | | | | | | | |
| | NoL | 1.000 | 1.000 | 1.000 | <0.01* | 1.000 | <0.01* | 1.000 | 1.000 | 0.970 | 1.000 | 1.000 | | | | | | | | | | | | | | |
| Msy | L | 1.000 | 1.000 | 1.000 | <0.01* | 1.000 | <0.01* | 1.000 | 1.000 | 0.843 | 1.000 | 1.000 | 1.000 | | | | | | | | | | | | | |
| | NoL | 1.000 | <0.01* | <0.01* | 1.000 | 0.012 | 1.000 | 0.263 | 1.000 | 1.000 | <0.01* | 1.000 | <0.01* | <0.01* | | | | | | | | | | | | |
| Mto | L | 1.000 | 0.843 | 1.000 | 1.000 | 1.000 | 1.000 | 1.000 | 1.000 | 1.000 | 0.730 | 1.000 | 0.632 | 1.000 | 1.000 | | | | | | | | | | | |
| | NoL | 0.730 | 1.000 | 1.000 | <0.01* | 1.000 | <0.01* | 1.000 | 1.000 | 0.632 | 1.000 | 1.000 | 1.000 | 1.000 | <0.01* | 0.402 | | | | | | | | | | |
| Mo | L | 1.000 | 1.000 | 1.000 | 0.015 | 1.000 | <0.01* | 1.000 | 1.000 | 1.000 | 1.000 | 1.000 | 1.000 | 1.000 | 0.010 | 1.000 | 1.000 | | | | | | | | | |
| | NoL | 1.000 | <0.01* | 0.012 | 1.000 | <0.01* | 1.000 | 0.177 | 0.808 | 1.000 | <0.01* | 1.000 | <0.01* | <0.01* | 1.000 | 1.000 | <0.01* | <0.01* | | | | | | | | |
| Ng | L | 1.000 | 1.000 | 1.000 | <0.01* | 1.000 | <0.01* | 1.000 | 1.000 | 1.000 | 1.000 | 1.000 | 1.000 | 1.000 | <0.01* | 1.000 | 1.000 | 1.000 | <0.01* | | | | | | | |
| | NoL | 1.000 | <0.01* | <0.01* | 1.000 | <0.01* | 1.000 | 0.141 | 1.000 | 1.000 | <0.01* | 1.000 | <0.01* | <0.01* | 1.000 | 1.000 | <0.01* | <0.01* | 1.000 | <0.01* | | | | | | |
| Pt | L | 1.000 | 1.000 | 1.000 | 0.123 | 1.000 | 0.074 | 1.000 | 1.000 | 1.000 | 1.000 | 1.000 | 1.000 | 1.000 | 0.179 | 1.000 | 1.000 | 1.000 | 0.087 | 1.000 | 0.079 | | | | | |
| | NoL | 1.000 | 1.000 | 1.000 | 1.000 | 1.000 | 0.282 | 1.000 | 1.000 | 1.000 | 0.771 | 1.000 | 1.000 | 1.000 | 1.000 | 1.000 | 0.838 | 1.000 | 0.308 | 1.000 | 0.464 | 1.000 | | | | |
| Ph | L | 1.000 | 1.000 | 1.000 | 0.518 | 1.000 | 0.216 | 1.000 | 1.000 | 1.000 | 1.000 | 1.000 | 1.000 | 1.000 | 0.664 | 1.000 | 1.000 | 1.000 | 0.309 | 1.000 | 0.309 | 1.000 | 1.000 | | | |
| | NoL | 1.000 | 1.000 | 1.000 | 1.000 | 1.000 | 1.000 | 1.000 | 1.000 | 1.000 | 1.000 | 1.000 | 1.000 | 1.000 | 1.000 | 1.000 | 1.000 | 1.000 | 1.000 | 1.000 | 1.000 | 1.000 | 1.000 | 1.000 | | |
| Ssy | L | 1.000 | 1.000 | 1.000 | 1.000 | 1.000 | 1.000 | 1.000 | 1.000 | 1.000 | 0.545 | 1.000 | 1.000 | 1.000 | 1.000 | 1.000 | 0.402 | 1.000 | 1.000 | 1.000 | 1.000 | 1.000 | 1.000 | 1.000 | 1.000 | |

| | | | | | | | | | | | | | | | | | | | | | | | | | | |
|---|---|---|---|---|---|---|---|---|---|---|---|---|---|---|---|---|---|---|---|---|---|---|---|---|---|---|
| | NoL | 1.000 | 1.000 | 1.000 | <0.01* | 1.000 | 0.000 | 1.000 | 1.000 | 0.843 | 1.000 | 1.000 | 1.000 | 1.000 | 0.000 | 0.970 | 1.000 | 1.000 | <0.01* | 1.000 | <0.01* | 1.000 | 1.000 | 1.000 | 1.000 | 1.000 |

**SI Table 5.** Results of the Bonferroni post-hoc with (L) and without (NoL) *labrum* in the 3D sample. Taxon abbreviations: Hs, *Homo sapiens*; Pt, *Pan troglodytes*; Hl, *Hylobates lar*; Ng, *Nomascus gabriellae*; Ssy, *Symphalangus syndactylus*; Ph, *Papio hamadryas*; Mto, *Macaca tonkeana*; Msi, *Macaca silenus*; Msy, *Macaca sylvanus*; Ca, *Chlorocebus aethiops*; Cal, *Cercocebus atys lunulatus*; Mo, *Miopithecus ogouensis*; Cas, *Cercopithecus ascanius*.

| | | Cal | | Cas | | Ca | | Hs | | Hl | | Mo | | Ng | | Pt | | Ph |
|---|---|---|---|---|---|---|---|---|---|---|---|---|---|---|---|---|---|---|
| | | L | NoL | L | NoL | L | NoL | L | NoL | L | NoL | L | NoL | L | NoL | L | NoL | L |
| Cal | NoL | 1.000 | | | | | | | | | | | | | | | | |
| Cas | L | 1.000 | 1.000 | | | | | | | | | | | | | | | |
| | NoL | 1.000 | 1.000 | 1.000 | | | | | | | | | | | | | | |
| Ca | L | 1.000 | 1.000 | 1.000 | 1.000 | | | | | | | | | | | | | |
| | NoL | 1.000 | 1.000 | 1.000 | 1.000 | 1.000 | | | | | | | | | | | | |
| Hs | L | 1.000 | 1.000 | 1.000 | 1.000 | 1.000 | 1.000 | | | | | | | | | | | |
| | NoL | 1.000 | 1.000 | 1.000 | 1.000 | 1.000 | 1.000 | 1.000 | | | | | | | | | | |
| Hl | L | 1.000 | 1.000 | 1.000 | 1.000 | 1.000 | 1.000 | 1.000 | 1.000 | | | | | | | | | |
| | NoL | 1.000 | 1.000 | 1.000 | 1.000 | 1.000 | 1.000 | 1.000 | 1.000 | 1.000 | | | | | | | | |
| Mo | L | 1.000 | 1.000 | 1.000 | 1.000 | 1.000 | 1.000 | 1.000 | 1.000 | 1.000 | 1.000 | | | | | | | |
| | NoL | 1.000 | 1.000 | 1.000 | 1.000 | 1.000 | 1.000 | 1.000 | 1.000 | 1.000 | 1.000 | 1.000 | | | | | | |
| Ng | L | 1.000 | 1.000 | 1.000 | 1.000 | 1.000 | 1.000 | 1.000 | 1.000 | 1.000 | 1.000 | 1.000 | 1.000 | | | | | |
| | NoL | 1.000 | 1.000 | 1.000 | 1.000 | 1.000 | 1.000 | 1.000 | 1.000 | 1.000 | 1.000 | 1.000 | 1.000 | 1.000 | | | | |
| Pt | L | 1.000 | 1.000 | 1.000 | 1.000 | 1.000 | 1.000 | 1.000 | 1.000 | 1.000 | 1.000 | 1.000 | 1.000 | 1.000 | 1.000 | | | |
| | NoL | 1.000 | 1.000 | 1.000 | 1.000 | 1.000 | 1.000 | 1.000 | 1.000 | 1.000 | 1.000 | 1.000 | 1.000 | 1.000 | 1.000 | 1.000 | | |
| Ph | L | 1.000 | 1.000 | 1.000 | 1.000 | 1.000 | 1.000 | 1.000 | 1.000 | 1.000 | 1.000 | 1.000 | 1.000 | 1.000 | 1.000 | 1.000 | 1.000 | |
| | NoL | 1.000 | 1.000 | 1.000 | 1.000 | 1.000 | 1.000 | 1.000 | 1.000 | 1.000 | 1.000 | 1.000 | 1.000 | 1.000 | 1.000 | 1.000 | 1.000 | 1.000 |

# Figures

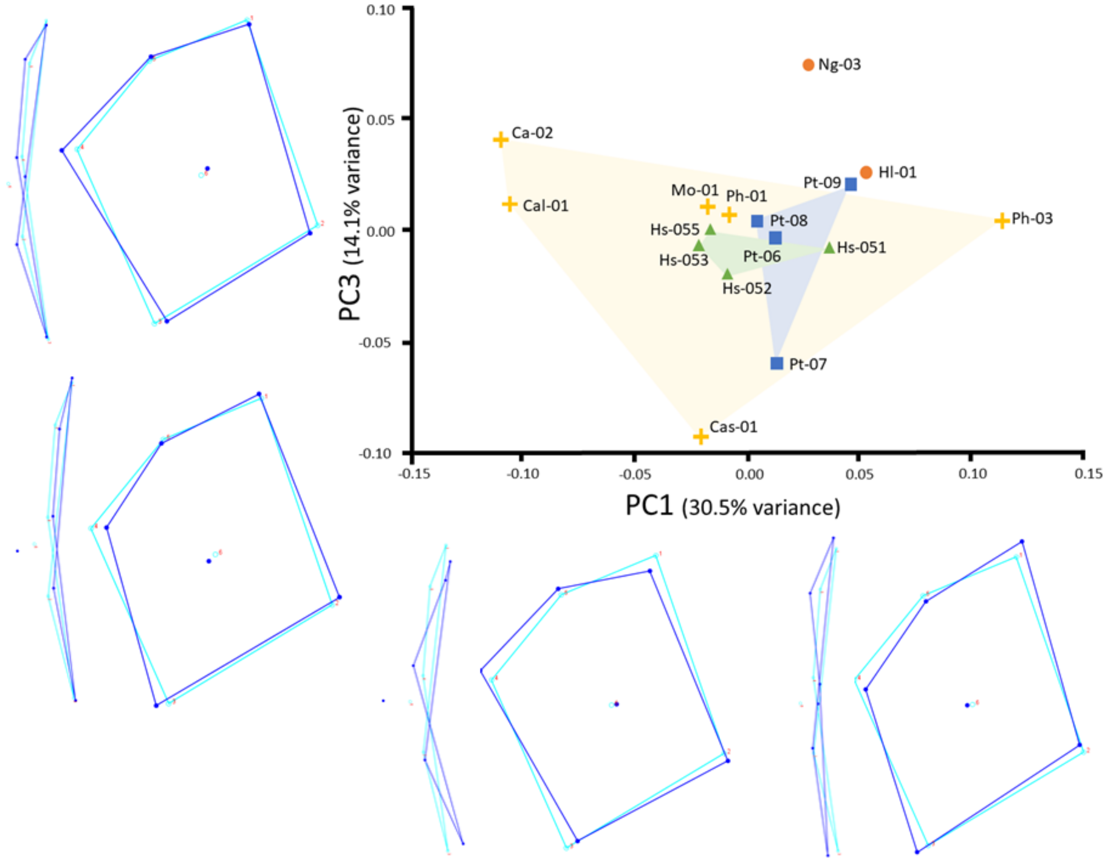

**SI Figure 1**. PC1 (30.5% of variance) vs PC3 (14.1% of variance) plot for the 3D geometric morphometric analysis of the glenoid without *labrum.* No discernable pattern or meaningful group separation was found. Wireframes represent the shape of the outline of the glenoid cavity in anterior (frontal) and side view at the end of each axis. Dark blue wireframes represent the target shape at the end of the axis and light blue wireframes represent the starting shape of the axis. Taxon abbreviations: Hs, *Homo sapiens*; Pt, *Pan troglodytes*; Hl, *Hylobates lar*; Ng, *Nomascus gabriellae*; Ssy, *Symphalangus syndactylus*; Ph, *Papio hamadryas*; Mto, *Macaca tonkeana*; Msi, *Macaca silenus*; Msy, *Macaca sylvanus*; Ca, *Chlorocebus aethiops*; Cal, *Cercocebus atys lunulatus*; Mo, *Miopithecus ogouensis*; Cas, *Cercopithecus ascanius*.

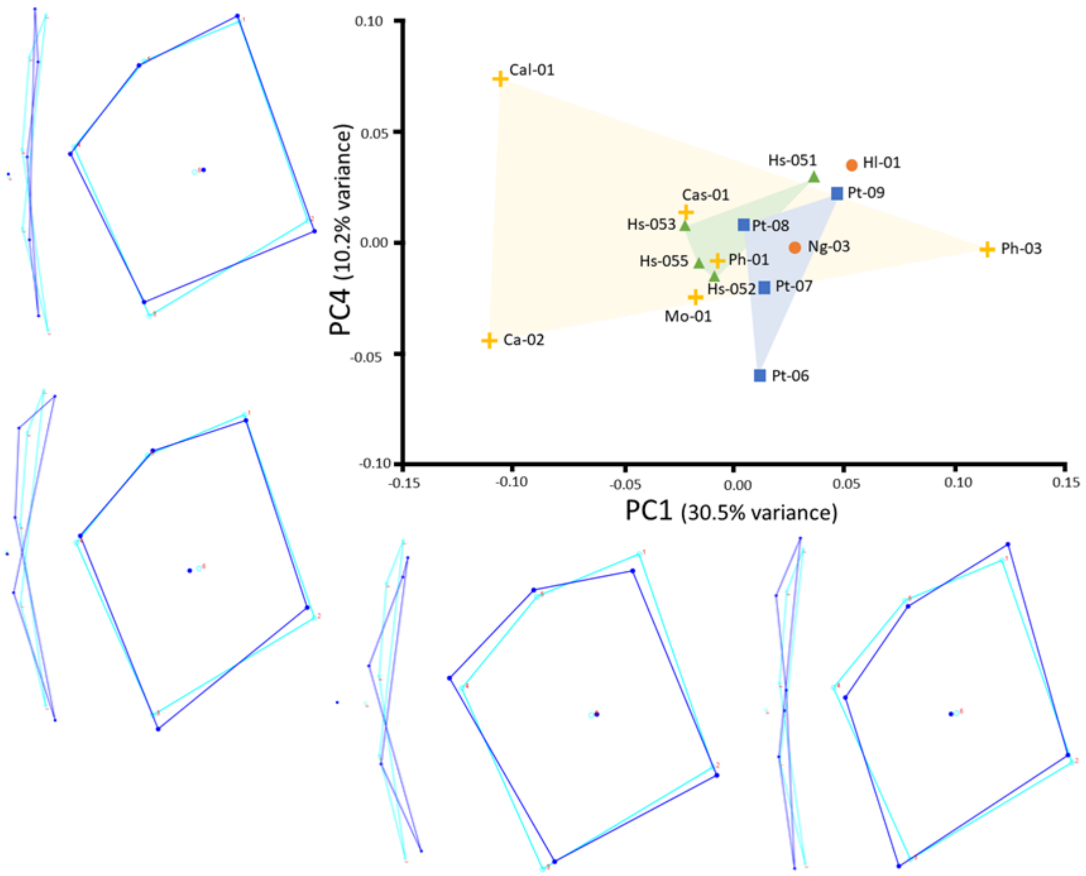

**SI Figure 2.** PC1 (30.5% of variance) vs PC4 (10.2% of variance) plot for the 3D geometric morphometric analysis of the glenoid without *labrum*. No discernable pattern or meaningful group separation was found. Wireframes represent the shape of the outline of the glenoid cavity in anterior (frontal) and side view at the end of each axis. Dark blue wireframes represent the target shape at the end of the axis and light blue wireframes represent the starting shape of the axis. Taxon abbreviations: Hs, *Homo sapiens*; Pt, *Pan troglodytes*; Hl, *Hylobates lar*; Ng, *Nomascus gabriellae*; Ssy, *Symphalangus syndactylus*; Ph, *Papio hamadryas*; Mto, *Macaca tonkeana*; Msi, *Macaca silenus*; Msy, *Macaca sylvanus*; Ca, *Chlorocebus aethiops*; Cal, *Cercocebus atys lunulatus*; Mo, *Miopithecus ogouensis*; Cas, *Cercopithecus ascanius*.

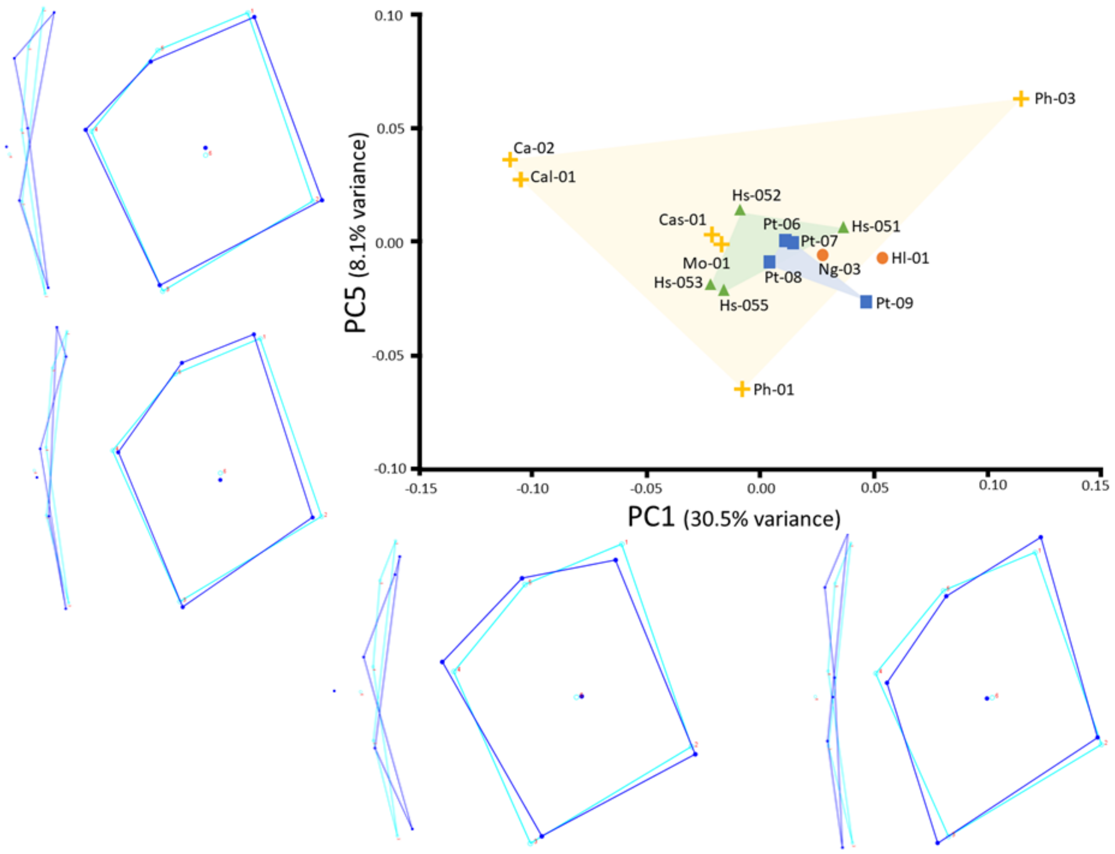

**SI Figure 3.** PC1 (30.5% of variance) vs PC5 (8.1% of variance) plot for the 3D geometric morphometric analysis of the glenoid without *labrum*. No discernable pattern or meaningful group separation was found. Wireframes represent the shape of the outline of the glenoid cavity in anterior (frontal) and side view at the end of each axis. Dark blue wireframes represent the target shape at the end of the axis and light blue wireframes represent the starting shape of the axis. Taxon abbreviations: Hs, *Homo sapiens*; Pt, *Pan troglodytes*; Hl, *Hylobates lar*; Ng, *Nomascus gabriellae*; Ssy, *Symphalangus syndactylus*; Ph, *Papio hamadryas*; Mto, *Macaca tonkeana*; Msi, *Macaca silenus*; Msy, *Macaca sylvanus*; Ca, *Chlorocebus aethiops*; Cal, *Cercocebus atys lunulatus*; Mo, *Miopithecus ogouensis*; Cas, *Cercopithecus ascanius*.

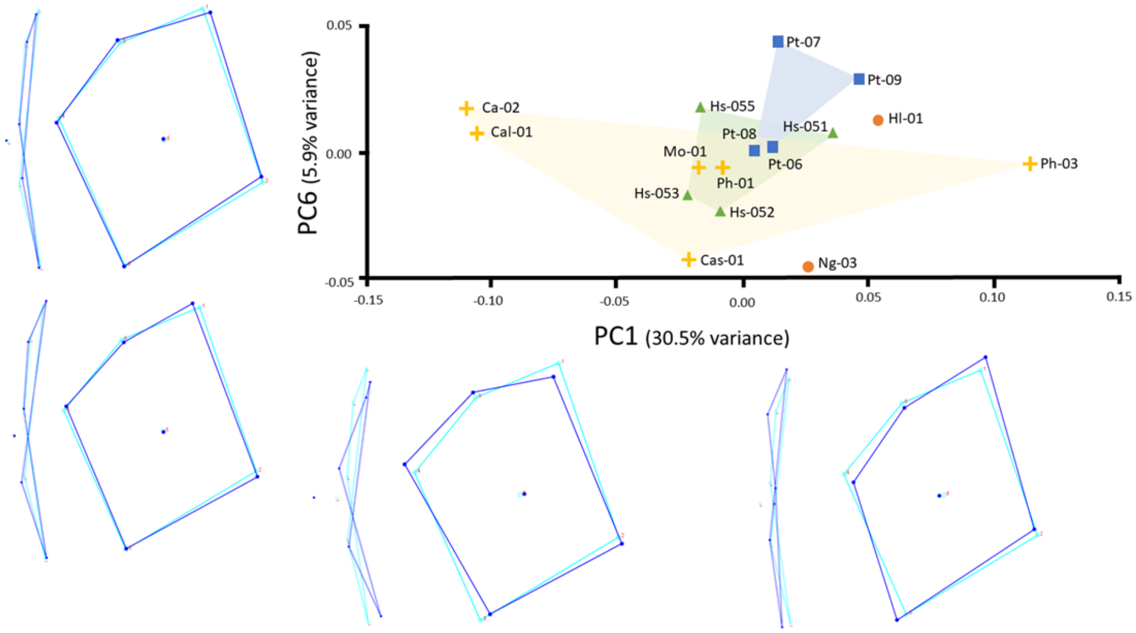

**SI Figure 4.** PC1 (30.5.% of variance) vs PC6 (5.8% of variance) plot for the 3D geometric morphometric analysis of the glenoid without *labrum*. No discernable pattern or meaningful group separation was found. Wireframes represent the shape of the outline of the glenoid cavity in anterior (frontal) and side view at the end of each axis. Dark blue wireframes represent the target shape at the end of the axis and light blue wireframes represent the starting shape of the axis. Taxon abbreviations: Hs, *Homo sapiens*; Pt, *Pan troglodytes*; Hl, *Hylobates lar*; Ng, *Nomascus gabriellae*; Ssy, *Symphalangus syndactylus*; Ph, *Papio hamadryas*; Mto, *Macaca tonkeana*; Msi, *Macaca silenus*; Msy, *Macaca sylvanus*; Ca, *Chlorocebus aethiops*; Cal, *Cercocebus atys lunulatus*; Mo, *Miopithecus ogouensis*; Cas, *Cercopithecus ascanius*.

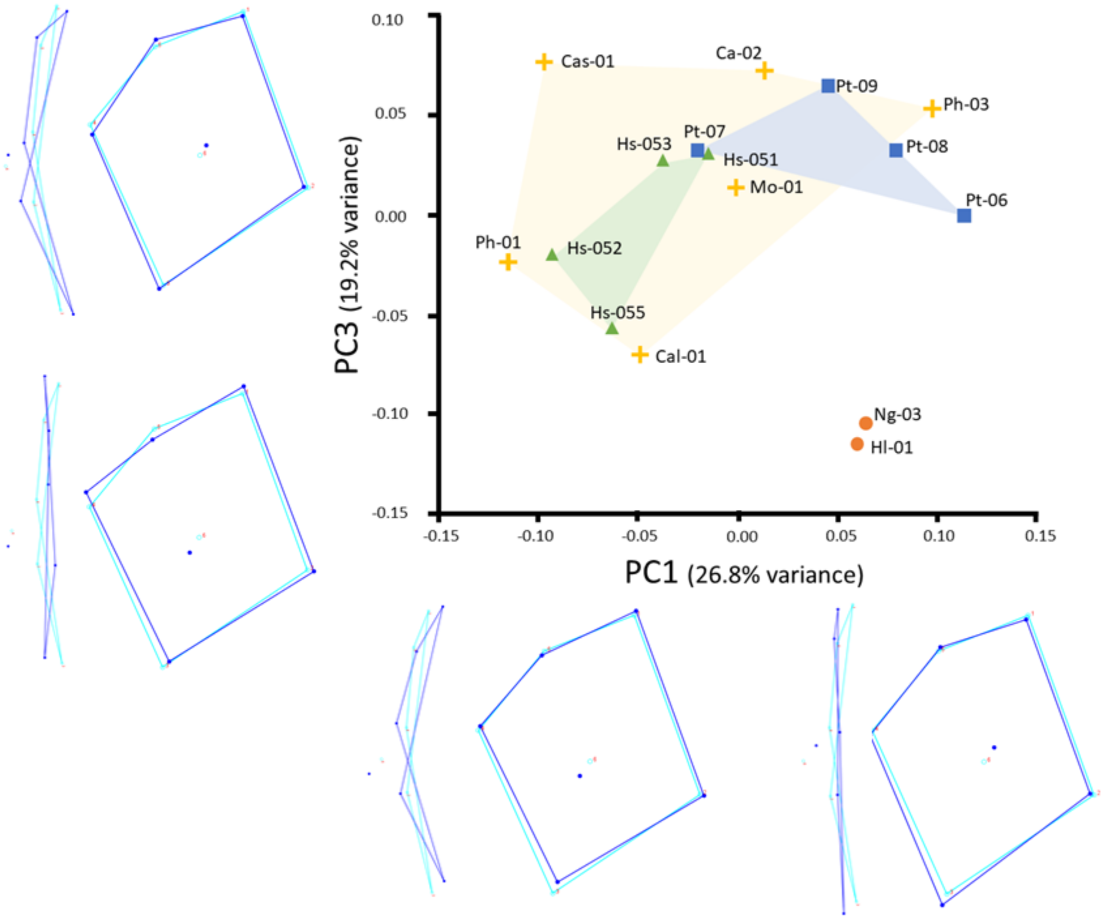

**SI Figure 5.** PC1 (26.8% of variance) vs PC3 (19.2% of variance) plot for the 3D geometric morphometric analysis of the glenoid with *labrum*. Group separation was found between hylobatids and the other groups. Wireframes represent the shape of the outline of the glenoid cavity in anterior (frontal) and side view at the end of each axis. Dark blue wireframes represent the target shape at the end of the axis and light blue wireframes represent the starting shape of the axis. Taxon abbreviations: Hs, *Homo sapiens*; Pt, *Pan troglodytes*; Hl, *Hylobates lar*; Ng, *Nomascus gabriellae*; Ssy, *Symphalangus syndactylus*; Ph, *Papio hamadryas*; Mto, *Macaca tonkeana*; Msi, *Macaca silenus*; Msy, *Macaca sylvanus*; Ca, *Chlorocebus aethiops*; Cal, *Cercocebus atys lunulatus*; Mo, *Miopithecus ogouensis*; Cas, *Cercopithecus ascanius*.

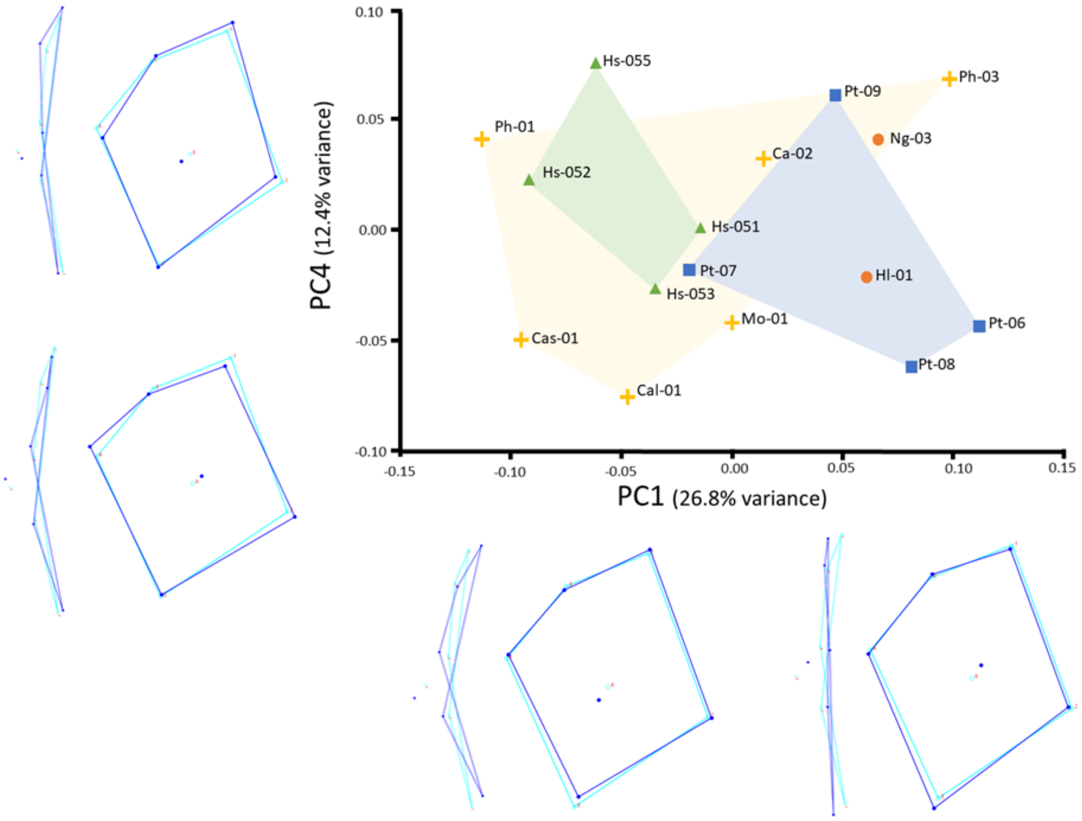

**SI Figure 6.** PC1 (26.8% of variance) vs PC4 (12.4% of variance) plot for the 3D geometric morphometric analysis of the glenoid with *labrum*. No discernable pattern or meaningful group separation was found. Wireframes represent the shape of the outline of the glenoid cavity in anterior (frontal) and side view at the end of each axis. Dark blue wireframes represent the target shape at the end of the axis and light blue wireframes represent the starting shape of the axis. Taxon abbreviations: Hs, *Homo sapiens*; Pt, *Pan troglodytes*; Hl, *Hylobates lar*; Ng, *Nomascus gabriellae*; Ssy, *Symphalangus syndactylus*; Ph, *Papio hamadryas*; Mto, *Macaca tonkeana*; Msi, *Macaca silenus*; Msy, *Macaca sylvanus*; Ca, *Chlorocebus aethiops*; Cal, *Cercocebus atys lunulatus*; Mo, *Miopithecus ogouensis*; Cas, *Cercopithecus ascanius*.

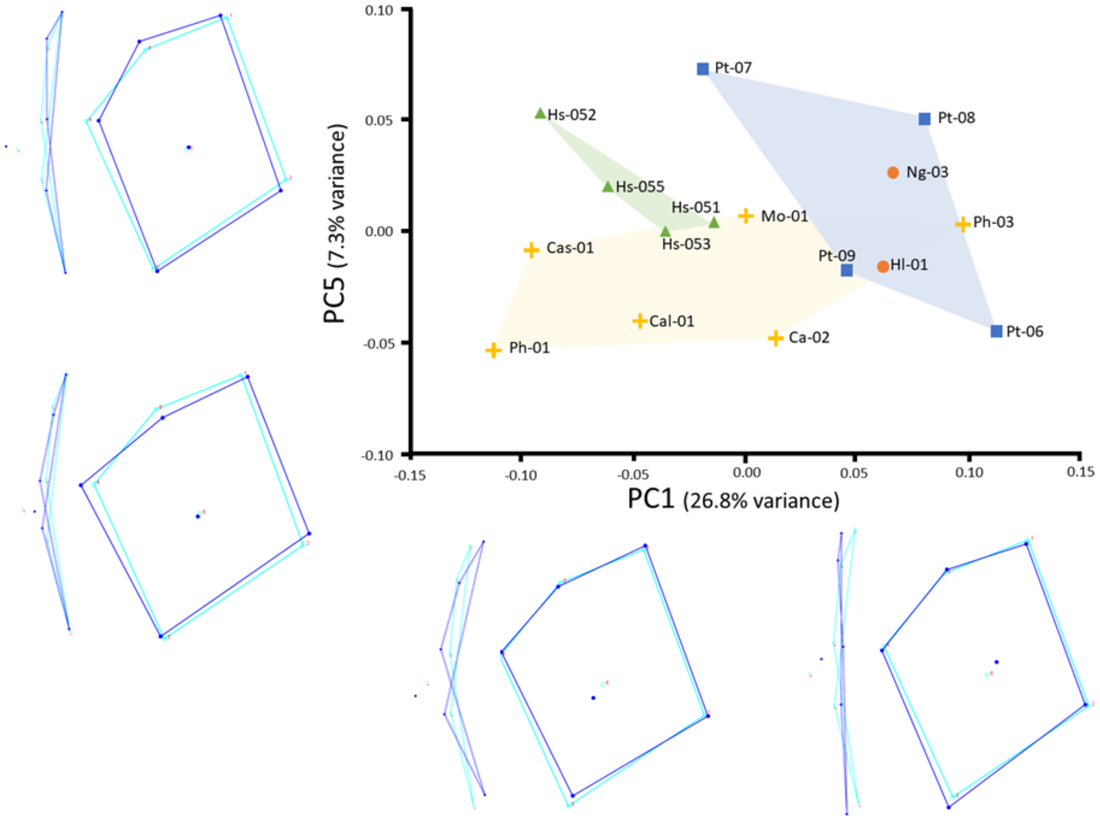

**SI Figure 7.** PC1 (26.8% of variance) vs PC5 (7.3 % of variance) plot for the 3D geometric morphometric analysis of the glenoid with *labrum.* No discernable pattern or meaningful group separation was found. Wireframes represent the shape of the outline of the glenoid cavity in anterior (frontal) and side view at the end of each axis. Dark blue wireframes represent the target shape at the end of the axis and light blue wireframes represent the starting shape of the axis. Taxon abbreviations: Hs, *Homo sapiens*; Pt, *Pan troglodytes*; Hl, *Hylobates lar*; Ng, *Nomascus gabriellae*; Ssy, *Symphalangus syndactylus*; Ph, *Papio hamadryas*; Mto, *Macaca tonkeana*; Msi, *Macaca silenus*; Msy, *Macaca sylvanus*; Ca, *Chlorocebus aethiops*; Cal, *Cercocebus atys lunulatus*; Mo, *Miopithecus ogouensis*; Cas, *Cercopithecus ascanius*.

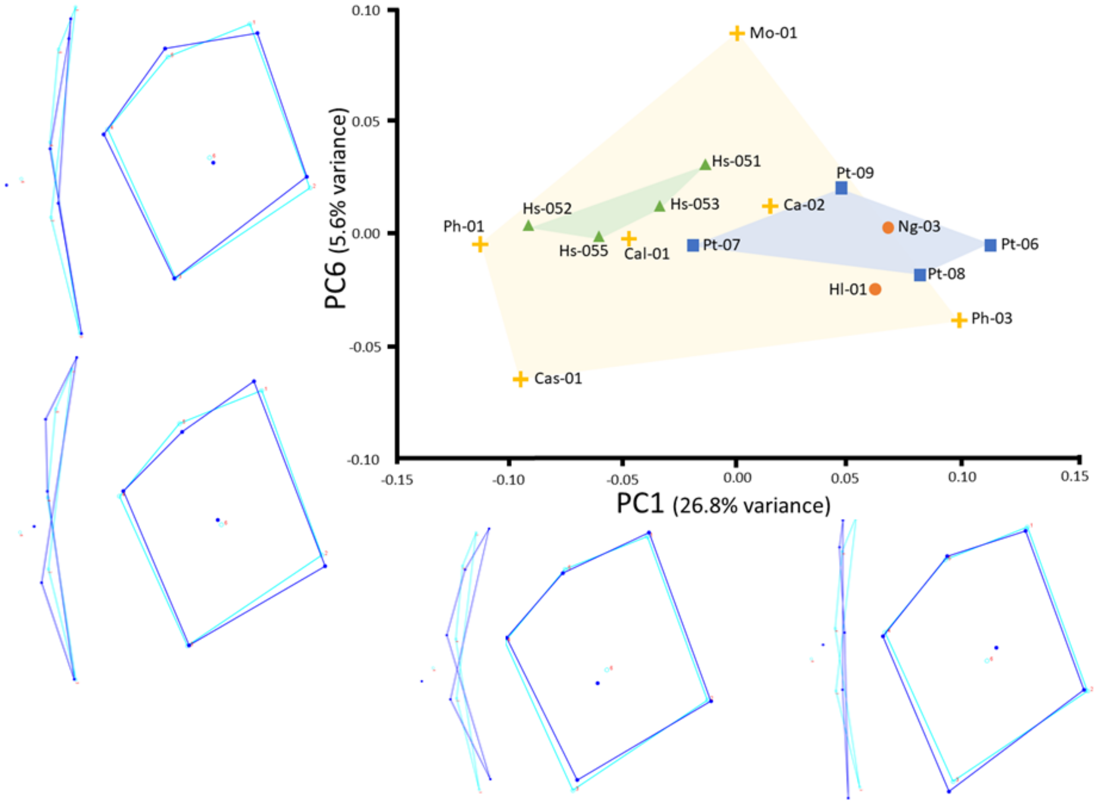

**SI Figure 8.** PC1 (26.8% of variance) vs PC6 (5.5% of variance) plot for the 3D geometric morphometric analysis of the glenoid with *labrum.* No discernable pattern or meaningful group separation was found. Wireframes represent the shape of the outline of the glenoid cavity in anterior (frontal) and side view at the end of each axis. Dark blue wireframes represent the target shape at the end of the axis and light blue wireframes represent the starting shape of the axis. Taxon abbreviations: Hs, *Homo sapiens*; Pt, *Pan troglodytes*; Hl, *Hylobates lar*; Ng, *Nomascus gabriellae*; Ssy, *Symphalangus syndactylus*; Ph, *Papio hamadryas*; Mto, *Macaca tonkeana*; Msi, *Macaca silenus*; Msy, *Macaca sylvanus*; Ca, *Chlorocebus aethiops*; Cal, *Cercocebus atys lunulatus*; Mo, *Miopithecus ogouensis*; Cas, *Cercopithecus ascanius*.

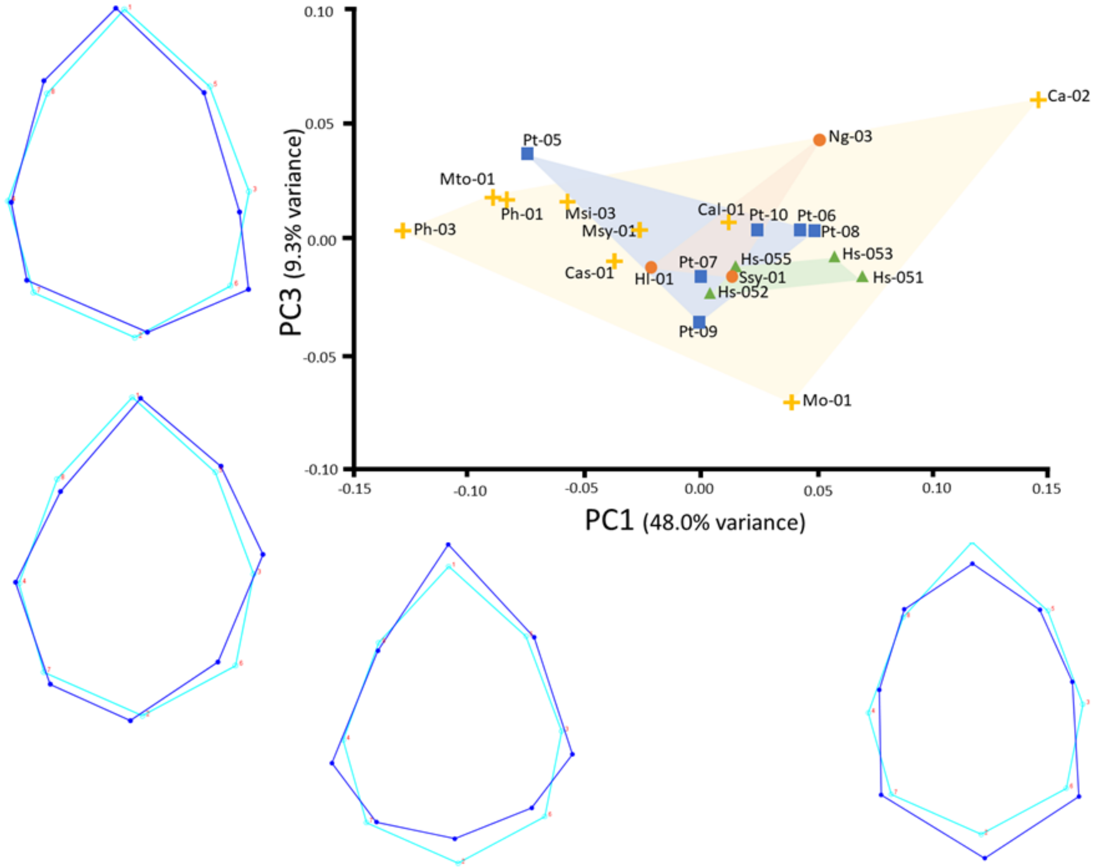

**SI Figure 9.** PC1 (48.0% of variance) vs PC3 (9.3% variance) plot for the 2D geometric morphometric analysis of the glenoid without *labrum*. No discernable pattern or meaningful group separation was found. Wireframes represent the shape of the outline of the glenoid cavity in anterior (frontal) view at the end of each axis. Dark blue wireframes represent the target shape at the end of the axis and light blue wireframes represent the starting shape of the axis. Taxon abbreviations: Hs, *Homo sapiens*; Pt, *Pan troglodytes*; Hl, *Hylobates lar*; Ng, *Nomascus gabriellae*; Ssy, *Symphalangus syndactylus*; Ph, *Papio hamadryas*; Mto, *Macaca tonkeana*; Msi, *Macaca silenus*; Msy, *Macaca sylvanus*; Ca, *Chlorocebus aethiops*; Cal, *Cercocebus atys lunulatus*; Mo, *Miopithecus ogouensis*; Cas, *Cercopithecus ascanius*.

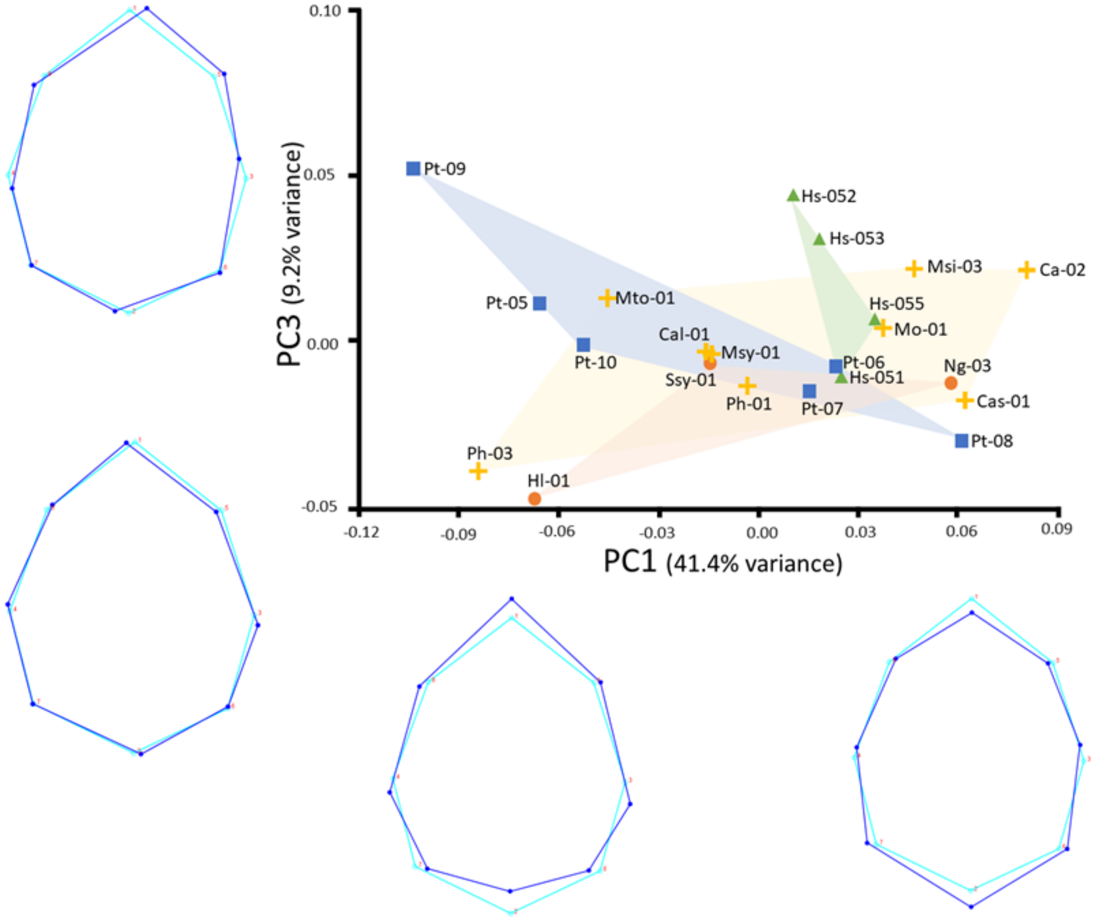

**SI Figure 10.** PC1 (41.4% of variance) vs PC3 (9.2% of variance) plot for the 2D geometric morphometric analysis of the glenoid with *labrum.* No discernable pattern or meaningful group separation was found. Wireframes represent the shape of the outline of the glenoid cavity in anterior (frontal) view at the end of each axis. Dark blue wireframes represent the target shape at the end of the axis and light blue wireframes represent the starting shape of the axis. Taxon abbreviations: Hs, *Homo sapiens*; Pt, *Pan troglodytes*; Hl, *Hylobates lar*; Ng, *Nomascus gabriellae*; Ssy, *Symphalangus syndactylus*; Ph, *Papio hamadryas*; Mto, *Macaca tonkeana*; Msi, *Macaca silenus*; Msy, *Macaca sylvanus*; Ca, *Chlorocebus aethiops*; Cal, *Cercocebus atys lunulatus*; Mo, *Miopithecus ogouensis*; Cas, *Cercopithecus ascanius*.

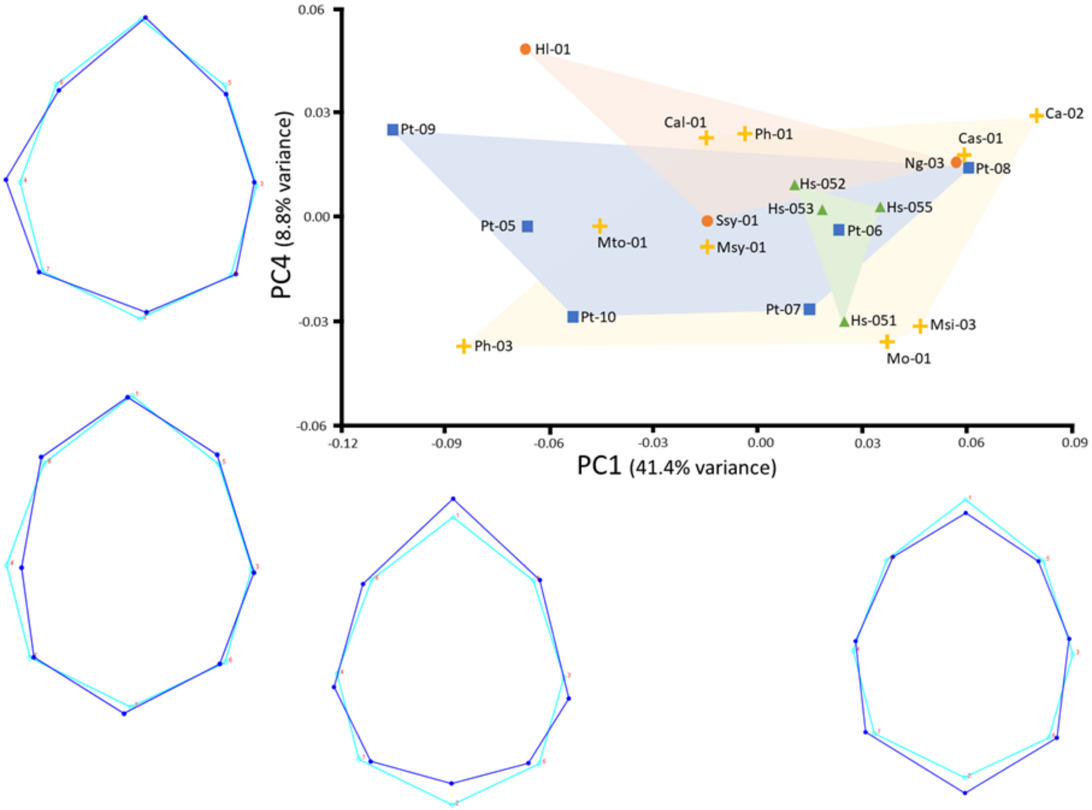

**SI Figure 11.** PC1 (41.4% of variance) vs PC4 (8.8% of variance) plot for the 2D geometric morphometric analysis of the glenoid with *labrum*. No discernable pattern or meaningful group separation was found. Wireframes represent the shape of the outline of the glenoid cavity in anterior (frontal) view at the end of each axis. Dark blue wireframes represent the target shape at the end of the axis and light blue wireframes represent the starting shape of the axis. Taxon abbreviations: Hs, *Homo sapiens*; Pt, *Pan troglodytes*; Hl, *Hylobates lar*; Ng, *Nomascus gabriellae*; Ssy, *Symphalangus syndactylus*; Ph, *Papio hamadryas*; Mto, *Macaca tonkeana*; Msi, *Macaca silenus*; Msy, *Macaca sylvanus*; Ca, *Chlorocebus aethiops*; Cal, *Cercocebus atys lunulatus*; Mo, *Miopithecus ogouensis*; Cas, *Cercopithecus ascanius*.

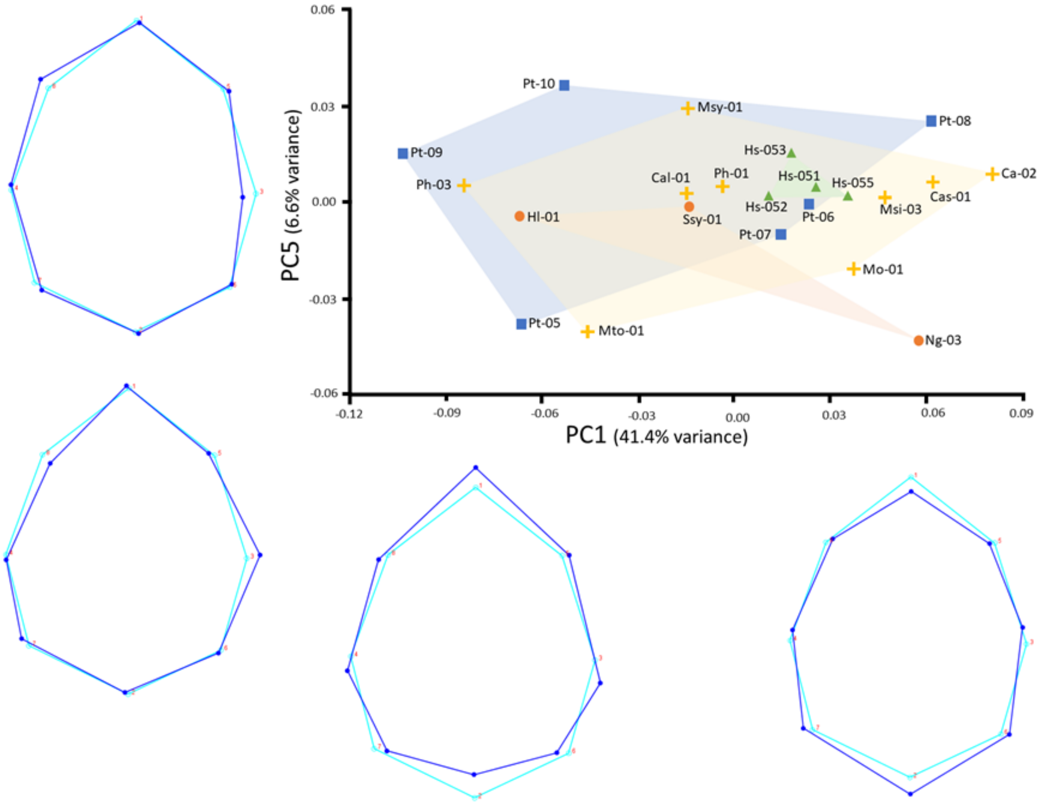

**SI Figure 12.** PC1 (41.4% of variance) vs PC5 (6.6% of variance) plot for the 2D geometric morphometric analysis of the glenoid with *labrum.* No discernable pattern or meaningful group separation was found. Wireframes represent the shape of the outline of the glenoid cavity in anterior (frontal) view at the end of each axis. Dark blue wireframes represent the target shape at the end of the axis and light blue wireframes represent the starting shape of the axis. Taxon abbreviations: Hs, *Homo sapiens*; Pt, *Pan troglodytes*; Hl, *Hylobates lar*; Ng, *Nomascus gabriellae*; Ssy, *Symphalangus syndactylus*; Ph, *Papio hamadryas*; Mto, *Macaca tonkeana*; Msi, *Macaca silenus*; Msy, *Macaca sylvanus*; Ca, *Chlorocebus aethiops*; Cal, *Cercocebus atys lunulatus*; Mo, *Miopithecus ogouensis*; Cas, *Cercopithecus ascanius*.